BIOCHEMISTRY
including biophysical chemistry & molecular biology

Article

pubs.acs.org/biochemistry

Phosphatidylinositol 3,4,5-Trisphosphate Activity Probes for the Labeling and Proteomic Characterization of Protein Binding Partners

Meng M. Rowland,[†] Heidi E. Bostic,[†] Denghuang Gong,[†] Anna E. Speers,[‡] Nathan Lucas,[§] Wonhwa Cho,[§] Benjamin F. Cravatt,[‡] and Michael D. Best*[,†]

[†]Department of Chemistry, University of Tennessee, 1420 Circle Drive, Knoxville, Tennessee 37996, United States

[‡]The Skaggs Institute for Chemical Biology and Department of Chemical Physiology, The Scripps Research Institute, La Jolla, California 92037, United States

[§]Department of Chemistry, University of Illinois at Chicago, 845 West Taylor Street, Chicago, Illinois 60607-7061, United States

Supporting Information

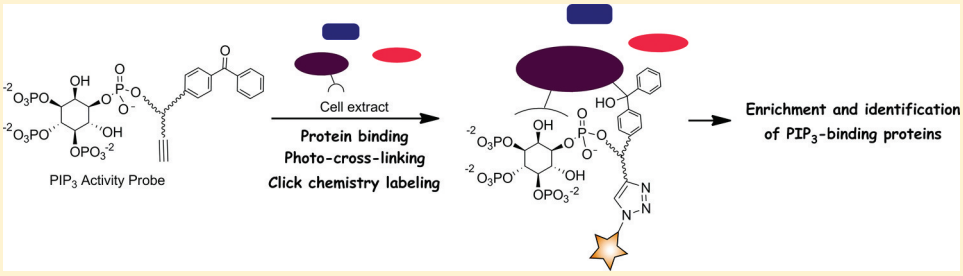

ABSTRACT: Phosphatidylinositol polyphosphate lipids, such as phosphatidylinositol 3,4,5-trisphosphate [PI(3,4,5)P_3], regulate critical biological processes, many of which are aberrant in disease. These lipids often act as site-specific ligands in interactions that enforce membrane association of protein binding partners. Herein, we describe the development of bifunctional activity probes corresponding to the headgroup of PI(3,4,5)P_3 that are effective for identifying and characterizing protein binding partners from complex samples, namely cancer cell extracts. These probes contain both a photoaffinity tag for covalent labeling of target proteins and a secondary handle for subsequent detection or manipulation of labeled proteins. Probes bearing different secondary tags were exploited, either by direct attachment of a fluorescent dye for optical detection or by using an alkyne that can be derivatized after protein labeling via click chemistry. First, we describe the design and modular synthetic strategy used to generate multiple probes with different reporter tags of use for characterizing probe-labeled proteins. Next, we report initial labeling studies using purified protein, the PH domain of Akt, in which probes were found to label this target, as judged by in-gel detection. Furthermore, protein labeling was abrogated by controls including competition with an unlabeled PI(3,4,5)P_3 headgroup analogue as well as through protein denaturation, indicating specific labeling. In addition, probes featuring linkers of different lengths between the PI(3,4,5)P_3 headgroup and photoaffinity tag led to variations in protein labeling, indicating that a shorter linker was more effective in this case. Finally, proteomic labeling studies were performed using cell extracts; labeled proteins were observed by in-gel detection and characterized using postlabeling with biotin, affinity chromatography, and identification via tandem mass spectrometry. These studies yielded a total of 265 proteins, including both known and novel candidate PI(3,4,5)P_3-binding proteins.

The phosphatidylinositol polyphosphates (PIP_ns), also known as the phosphoinositides, represent an important family of signaling lipids that control numerous key cellular processes.[1,2] These molecules contain a conserved *myo*-inositol headgroup that is attached via a phosphodiester linkage at position 1 to a glycerolipid backbone. The family consists of seven naturally occurring isomers that exhibit differential patterns of phosphorylation, specifically including every combination of phosphate groups at positions 3−5 of the *myo*-inositol headgroup. A primary activity of the PIP_ns is to serve as site-specific ligands in protein binding events that enforce protein−membrane association.[3,4] Because of the key roles of these lipids in regulating critical biological pathways, they have been linked to aberrant activities associated with diseases, including cancer and diabetes.[5−8] One of the most prominent links to disease involves the role of phosphatidylinositol 3,4,5-trisphosphate [PI(3,4,5)P_3] as a ligand for Akt (protein kinase B).[9−14] This binding event promotes association of Akt with the inner leaflet of the plasma membrane,[15] where it is then activated through multiple phosphorylation events. Activated Akt feeds into numerous pathways that promote cell survival, and thus, the enzymes that produce (phosphoinositide 3-kinase)[16] and hydrolyze (PTEN)[17] PI(3,4,5)P_3 are among the most commonly mutated enzymes in cancer.[18,19]

The understanding of PIP_n binding properties is hindered by complexity at multiple levels. Many proteins that bind PIP_ns contain at least one of a number of conserved binding module

Received: October 27, 2011
Published: November 10, 2011

sequences, such as the PH, PX, FYVE, ENTH, ANTH, FERM, Tubby, and PROPPIN domains, members of which can be identified by sequence homology searches. New domain families have continued to be discovered in recent years, and there are likely further as yet undiscovered PIP_n-targeting sequences. Furthermore, complexities often arise within domain families, such as with the PH domains, where only a fraction of family members bind PIP_ns, and those PH domain-containing proteins that do bind PIP_ns exhibit broad diversity in their specificities for particular PIP_n targets. Finally, other proteins that bind PIP_ns appear to lack any consensus binding sequence, making them more difficult to identify. As a result of these complexities, global methods for the identification and characterization of PIP_n-binding proteins are of significant interest.

The primary method that has been effectively employed for global characterization of PIP_n-binding proteins has involved affinity purification using solid supports decorated with different lipid motifs.[20−27] Affinity chromatography using PIP_n-functionalized beads was initially used to purify individual proteins,[28,29] and applications have since expanded as a result of advancements in the technology for identifying protein binding partners. In an early example, libraries of radiolabeled proteins were screened, which led to the identification of two known and one new target of different PIP_ns.[20] The scope of studies has expanded due to progress in mass spectrometry-based proteomic analysis, resulting in the identification of numerous PIP_n-binding proteins.[22,24−27,30] In a recent report, 282 PI(3,4,5)P_3-binding proteins were identified using beads decorated with this headgroup that were used directly for studies or through incorporation of the beads into liposomes to mimic the environment of cellular membranes.[25] In addition to affinity chromatography, proteome chips have also been used to probe protein−PIP_n binding interactions.[31] This was performed by immobilization of GST-tagged proteins from yeast, followed by microarray analysis of binding to biotin-labeled PIP_n-containing liposomes. One note regarding these proteomic analyses is that the exact set of proteins that has been identified has varied among the studies. This indicates that the specific conditions that are employed for analysis affect the results, suggesting that it will be beneficial to pursue diverse approaches to elucidate the full complement of PIP_n-binding proteins.

A strategy that shows great promise for broad and efficient characterization of lipid-binding proteins is activity-based protein profiling (ABPP),[32] in which protein targets are collectively characterized on the basis of function, in this case ligand binding properties. In this approach, target proteins are collectively labeled, purified, and characterized from complex biological samples such as cell extracts and live cells using small molecule probes that range from active site-directed analogues of enzyme substrates to derivatized versions of biologically active ligands. Recently, phospholipid-based activity probes have been applied to characterize both lipid-binding proteins[33,34] and lipid-modifying phospholipase enzymes[35] using synthetic analogues of phosphatidylcholine. A significant advantage of ABPP is that protein targets can be labeled in living cells, allowing for the probing of activities under normal physiological conditions, which is critical because proteins operate much differently in live cells and cell extracts. In addition, the covalent labeling of protein targets in ABPP circumvents the problem of noncovalent interactions falling apart during processing and enhances the likelihood of identifying protein targets that bind the probe with weaker affinities. Because of the benefits of ABPP, we set out to develop activity-based probes corresponding to the PIP_ns that are effective for proteomics toward their eventual use in live cell labeling studies.

EXPERIMENTAL PROCEDURES

General Experimental. Reagents were generally purchased from Acros, Aldrich, or Fisher Scientific and used as received. Dry solvents were obtained from a Pure Solv solvent delivery system purchased from Innovative Technology, Inc. Column chromatography was performed using 230−400 mesh silica gel purchased from Sorbent Technologies and a C18 (17%) reverse-phase column (6 mL, 2 g) purchased from Silicycle. NMR spectra were recorded using a Varian Mercury 300 spectrometer. Mass spectra were recorded with an ABI DE Pro MALDI spectrometer with high-resolution capabilities. Protein photo-cross-linking was performed using a Spectroline ENF260C UV lamp. Proteins were visualized in gel using a Hibachi FMBio lle flatbed laser-induced fluorescence scanner (MiraiBio, Alameda, CA). Dulbecco's phosphate-buffered saline (PBS) was purchased from Cellgro. Cell lines were purchased from ATCC. Heat-denatured proteins or cell extracts were generated by denaturation at 90 °C for 5 min. PIP_n headgroup−amine conjugates **4a** and **4b**,[36] azido-rhodamine **11**,[37] and THPTA[38] were each synthesized according to previously reported procedures. The GST-tagged PH domain of Akt was expressed and purified as previously reported.[39] Cancer cell extracts were prepared using a previously reported procedure.[37]

Synthesis of PIP_n Activity-Based Probes. *Benzophenone-Lys-OMe trifluoroacetate salt (**6**).* A reported procedure[40] was used to prepare compound **6**. Cbz-Lys(Boc)-OMe (**5**) (262 mg, 0.664 mmol) was dissolved in 5 mL of methanol, and palladium(II) hydroxide (26 mg, 10 wt %) was added to the solution. The reaction mixture was stirred under a hydrogen atmosphere overnight, and the reaction crude was then filtered through a pad of Celite. The filtrate was concentrated to yield Lys(Boc)-OMe, which was used in the next step without further purification. Lys(Boc)-OMe was dissolved in 10 mL of *N*,*N*-dimethylformamide, to which 4-benzoylbenzoic acid (150 mg, 0.664 mmol), *N*-[3-(dimethylamino)propyl]-*N*′-ethylcarbodiimide hydrochloride (EDCI, 153 mg, 0.797 mmol), 4-(dimethylamino)pyridine (DMAP, 97 mg, 0.791 mmol), and *N*-methylmorpholine (NMM, 0.26 mL, 2.32 mmol) were added. The solution was stirred at rt overnight and then concentrated under reduced pressure. The crude was purified by silica gel column chromatography with a 50% ethyl acetate/hexanes solvent system to yield benzophenone-Lys(Boc)-OMe as a white foam (279 mg, 90% over two steps). The characterization of benzophenone-Lys(Boc)-OMe matched the literature.[40] Benzophenone-Lys(Boc)-OMe (0.279 g, 0.595 mmol) was then dissolved in 4 mL of a trifluoroacetic acid/dichloromethane mixture (1:1, v/v). The reaction mixture was allowed to stir at rt for 2 h and then concentrated under reduced pressure to yield **6** as a yellowish gum (0.272 g, 100%): ^{1}H NMR (300 MHz, $CDCl_3$) δ 7.88 (d, J = 9 Hz, 1H), 7.70−7.67 (m, 4H), 7.57−7.52 (m, 2H), 7.44−7.40 (m, 2H), 4.67−4.65 (m, 1H), 3.66 (s, 3H), 2.89−2.87 (m, 2H), 1.86−1.64 (m, 4H), 1.46−1.43 (m, 2H); ^{13}C NMR (300 MHz, $CDCl_3$) δ 196.7, 172.6, 140.7, 136.7, 136.5, 133.4, 130.2, 130.1, 128.7, 127.5, 53.0, 52.8, 40.2, 31.3, 26.7, 22.4; MALDI-HRMS calcd for $[M + Na]^+$ 391.1634, found 391.1632.

*Benzophenone-Lys[5(6)-carboxyfluorescein]-OMe (**7a**).* Benzophenone-Lys-OMe (**6**, 175 mg, 0.475 mmol) was combined with 5(6)-carboxyfluorescein (197 mg, 0.522 mmol), *N*-[3-(dimethylamino)propyl]-*N*′-ethylcarbodiimide hydrochloride (EDCI, 118 mg, 0.618 mmol), 4-(dimethylamino)-pyridine (DMAP, 70 mg, 0.570 mmol), and *N*-methylmorpholine (NMM, 0.21 mL, 1.90 mmol) in 8 mL of dry *N*,*N*-dimethylformamide. The reaction mixture was allowed to stir at rt overnight, at which point the solvent was removed under reduced pressure. The crude was dissolved in 50 mL of a methanol/chloroform mixture (1:4, v/v) and extracted with 50 mL of a 2 N hydrochloric acid aqueous solution, and the aqueous layer was washed with 2 × 50 mL of a methanol/chloroform mixture (1:4, v/v). The organic layers were then combined, dried with magnesium sulfate, concentrated by rotary evaporation, and then purified using column chromatography with a 5 to 10% methanol/chloroform gradient solvent system to yield benzophenone-Lys[5(6)-carboxyfluorescein]-OMe (**7a**) as an orange solid (159 mg, 46%): ^{1}H NMR [300 MHz, CD_3OD/$CDCl_3$ (1:2, v/v)] δ 8.40−8.39 (m, 1H), 8.03−7.98 (m, 2H), 7.95−7.83 (m, 2H), 7.85−7.75 (m, 3H), 7.66−7.69 (m, 1H), 7.54−7.49 (m, 2H), 7.25−7.22 (m, 1H), 6.72−6.70 (m, 2H), 6.57−6.53 (m, 4H), 4.76−4.72 (m, 1H), 3.80 (s, 3H), 3.50−3.48 (m, 1H), 3.36−3.35 (m, 1H), 2.67 (bs, 1H), 2.06−1.94 (m, 2H), 1.74−1.46 (m, 4H); MALDI-HRMS calcd for $[M + Na]^+$ 749.2111, found 749.2165.

*Benzophenone-Lys[5(6)-carboxyfluorescein]-OH (**7b**).* Compound **7a** (36 mg, 0.050 mmol) was suspended in 5 mL of methanol. To this solution was added 5 mL of a 2 M sodium hydroxide aqueous solution, and the reaction mixture was stirred at rt for 10 min, followed by the addition of 30 mL of a 2 N hydrochloric acid aqueous solution. An orange solid was formed immediately upon addition of the acid, which was filtered and washed with 2 × 10 mL of a 2 N hydrochloric acid aqueous solution to yield crude **7b**. The crude was then dissolved in acetonitrile and water and purified on a C18 reverse-phase column (2 g) with a 0−80% acetonitrile/water gradient solvent system. Compound **7b** eluted with ∼45−60% acetonitrile/water solution. The collected fractions were concentrated by rotary evaporation to remove acetonitrile followed by lyophilization of the water to yield benzophenone-Lys[5(6)-carboxyfluorescein]-OH (**7b**) as a yellow powder (19 mg, 53%): ^{1}H NMR [300 MHz, CD_3CN/D_2O (1:1, v/v)] δ 8.73−8.71 (m, 1H), 8.42−8.29 (m, 4H), 8.14−8.07 (m, 4H), 7.92−7.87 (m, 2H), 7.53−7.50 (m, 1H), 7.10 (s, 2H), 6.97−6.93 (m, 4H), 4.95−4.85 (m, 1H), 3.82−3.80 (m, 1H), 3.67−3.65 (m, 1H), 2.40−2.38 (m, 2H), 1.94−1.80 (m, 4H); MALDI-HRMS calcd for $[M + H]^+$ 713.2130, found 713.2072.

*Benzophenone-Lys(alkyne)-OMe (**8a**).* Benzophenone-Lys-OMe (**6**, 911 mg, 1.890 mmol) was combined with alkyne **10** (293 mg, 1.89 mmol), *N*-[3-(dimethylamino)propyl]-*N*′-ethylcarbodiimide hydrochloride (EDCI, 543 mg, 2.83 mmol), 4-(dimethylamino)pyridine (DMAP, 346 mg, 2.83 mmol), and *N*-methylmorpholine (NMM, 2.08 mL, 18.9 mmol) in 10 mL of a methanol/chloroform mixture (1:4, v/v). The reaction mixture was allowed to stir at rt overnight, and the solvent was then removed under reduced pressure. The crude was purified by column chromatography with a 50 to 100% acetone/hexanes gradient solvent system to yield benzophenone-Lys(alkyne)-OMe (**8a**) as a colorless crystal (760 mg, 80%): ^{1}H NMR (300 MHz, $CDCl_3$) δ 7.99−7.96 (m, 2H), 7.81−7.75 (m, 3H), 7.61−7.57 (m, 1H), 7.50−7.42 (m, 3H), 6.81−6.79 (m, 1H), 6.55−6.51(m, 1H), 4.74−4.67 (m, 1H), 3.95−3.93 (m, 2H), 3.75 (s, 3H), 3.27−3.15 (m, 2H), 2.42−2.41 (m, 4H), 2.17−2.14 (m, 1H), 1.90−1.86 (m, 2H), 1.53−1.42 (m, 4H); MALDI-HRMS calcd for $[M + Na]^+$ 528.2105, found 528.2134.

*Benzophenone-Lys(alkyne)-OH (**8b**).* Compound **8a** (135 mg, 0.267 mmol) was dissolved in 10 mL of a methanol/ethanol mixture (1:1, v/v). To this solution was added 8 mL of a 2 M sodium hydroxide aqueous solution. The reaction mixture was stirred at rt for 15 min and then extracted from a 2 N hydrochloric acid aqueous solution (100 mL) with 200 mL of dichloromethane, and the aqueous layer was washed with 3 × 50 mL of a methanol/chloroform mixture (1:4, v/v). The combined organic layers were then dried with magnesium sulfate, filtered, and concentrated to yield benzophenone-Lys(alkyne)-OH (**8b**) as a white solid (94 mg, 72%): ^{1}H NMR (300 MHz, CD_3OD) δ 8.01−7.99 (m, 2H), 7.84−7.76 (m, 4H), 7.65−7.63 (m, 1H), 7.55−7.53 (m, 2H), 4.59−4.57 (m, 1H), 3.95−3.93 (m, 1H), 3.65−3.61 (m, 2H), 3.21−3.19 (m, 2H), 2.57−2.45 (m, 5H), 1.99.92 (m, 2H), 1.56−1.54 (m, 4H); ^{13}C NMR (300 MHz, $CDCl_3$) δ 196.2, 174.2, 171.9, 168.0, 140.0, 137.3, 136.8, 132.8, 129.7, 129.6, 128.3, 127.4, 78.2, 71.1, 53.1, 38.9, 30.6, 28.5, 28.2, 23.2, 21.4; MALDI-HRMS calcd for $[M + Na]^+$ 514.1954, found 514.1974.

*Benzophenone-Lys(alkyne)-hexanoate (**9a**).* Carboxylic acid **8b** (144 mg, 0.293 mmol) was combined with 6-aminocaproic acid methyl ester hydrochloride (69 mg, 0.381 mmol), *N*-[3-(dimethylamino)propyl]-*N*′-ethylcarbodiimide hydrochloride (EDCI, 72 mg, 0.381 mmol), 4-(dimethylamino)-pyridine (DMAP, 47 mg, 0.381 mmol), and *N*-methylmorpholine (NMM, 0.32 mL, 2.92 mmol) in 15 mL of a methanol/chloroform mixture (1:4, v/v). The reaction mixture was allowed to stir at rt overnight, and the solvent was then removed under reduced pressure. The crude was purified by column chromatography with a 50 to 100% acetone/hexanes gradient solvent system to yield compound **9a** as a colorless crystal (91 mg, 50%): ^{1}H NMR (300 MHz, $CDCl_3$) δ 8.00−7.97 (m, 2H), 7.83−7.77 (m, 4H), 7.64−7.59 (m, 1H), 7.52−7.47 (m, 2H), 7.21−7.19 (m, 1H), 6.83−6.81(m, 1H), 4.68−4.66 (m, 1H), 3.98−3.96 (m, 2H), 3.64 (s, 3H), 3.25−3.23 (m, 4H), 2.54−2.48 (m, 4H), 2.29 (t, J = 6 Hz, 2H), 2.21−2.18 (m, 1H), 1.92−1.83 (m, 2H), 1.62−1.34 (m, 10H); ^{13}C NMR (300 MHz, $CDCl_3$) δ 196.1, 174.1, 172.5, 172.4, 171.7, 166.8, 140.3, 136.9, 133.0, 130.1, 130.0, 128.5, 127.4, 79.7, 71.31, 53.7, 51.6, 39.4, 33.8, 31.3, 29.1, 26.3, 24.4, 22.8; MALDI-HRMS calcd for $[M + Na]^+$ 641.2951, found 641.2953.

*4-Oxo-4-(2-propyn-1-ylamino)butanoic Acid (**10**).*[41] Propargylamine (1.5 mL, 21.87 mmol) was dissolved in 10 mL of an *N*,*N*-dimethylformamide/acetonitrile mixture (1:1, v/v) at 0 °C. To this solution was added succinic anhydride (2.19 g, 21.87 mmol) in 10 mL of acetonitrile, and the resulting solution was stirred at rt overnight. Next, the solvent was removed under reduced pressure. The residue was then washed with hexanes and then ethyl ether to yield crude **10** as a brownish solid. The crude product was purified by column chromatography with a 50−75% ethyl acetate/hexanes solvent system to yield **10** as a pale yellowish solid (1.414 g, 42%): ^{1}H NMR (300 MHz, CD_3OD) δ 3.94 (d, J = 3 Hz, 1H), 2.61−2.56 (m, 2H), 2.49−2.44 (m, 2H); ^{13}C NMR (300 MHz, $CDCl_3$) δ 174.8, 172.7, 79.2, 70.8, 29.9, 28.7, 28.1; DART-HRMS calcd for $[M + H]^+$ 156.0661, found 156.0670.

*Benzophenone-Lys[5(6)-carboxyfluorescein]-PI(3,4)P$_2$ (**1**).* Acid **7b** (28 mg, 0.039 mmol) was dissolved in 4 mL of an *N*,*N*-dimethylformamide/tetrahydrofuran mixture (1:2, v/v). To this

stirred solution were added dicyclohexylcarbodiimide (DCC, 16 mg, 0.078 mmol) and then *N*-hydroxysuccinimide (9 mg, 0.078 mmol). The reaction mixture was stirred for 8 h at rt and then filtered. The filtrate was concentrated to ~0.5 mL, to which was added 50 mL of ethyl ether, after which an orange precipitate was formed and filtered. The solid was then dissolved in 10 mL of tetrahydrofuran and filtered. The filtrate was concentrated to yield the NHS ester of **7b**, which was moved to the next step without further purification. The resulting succinimidyl ester was dissolved in 1 mL of *N*,*N*-dimethylformamide, which was added to a solution of PI(3,4)P_2-amine **4a**[36] (10 mg, 0.019 mmol) in 1 mL of tetraethylammonium bicarbonate (TEAB, 1 M, pH 7.5) and 0.5 mL of tetrahydrofuran. The reaction mixture was allowed to stir at rt overnight, and the solvent was then removed under reduced pressure. The solid crude product was washed with acetone (3 × 20 mL) and then dissolved in deionized water to stir with 500 mg of Chelex 100, sodium form at rt for 2 h. The reaction solution was then directly loaded onto a C18 reverse-phase column (2 g), and the column was eluted with deionized water (20 mL). The water elution was lyophilized to yield **1** as a yellow solid (8.0 mg, 35%): ^{1}H NMR [300 MHz, CD_3OD/D_2O (1:1, v/v)] δ 7.75−7.00 (m, 12H), 6.55 (s, 2H), 6.30−6.28 (m, 2H), 5.89−5.86 (s, 2H), 4.30−4.28 (s, 2H), 4.02−3.98 (m, 2H), 3.72−3.31 (m, 14H), 1.53−1.04 (m, 14H); ^{31}P NMR [121.5 MHz, CD_3OD/D_2O (1:1, v/v)] δ 5.05, 3.64, 0.12; MALDI-HRMS calcd for $[M + H]^+$ 1214.2696, found 1214.7771.

*Benzophenone-Lys(alkyne)-PI(3,4,5)P_3 (**2**).* Acid **8b** (47 mg, 0.096 mmol) was dissolved in 5 mL of tetrahydrofuran. To this stirred solution were added *N*-[3-(dimethylamino)propyl]-*N*′-ethylcarbodiimide hydrochloride (EDCI, 37 mg, 0.192 mmol) and then *N*-hydroxysuccinimide (22 mg, 0.192 mmol). The reaction mixture was stirred for 8 h at rt and then concentrated. The crude was dissolved in 30 mL of chloroform and washed with water (3 × 20 mL). The organic layer was concentrated, and 30 mL of ethyl ether was added, after which the resulting white precipitate was filtered and redissolved in chloroform (15 mL). This solution was filtered, and the filtrate was concentrated to yield the crude NHS ester of **8b** as a colorless oil. The crude NHS ester was then stirred in 1 mL of *N*,*N*-dimethylformamide, to which was added **4b** (10 mg, 0.0167 mmol) in 1 mL of tetraethylammonium bicarbonate (TEAB, 1 M, pH 7.5). Additionally, 1 mL of tetrahydrofuran was added to enhance solubility. The reaction mixture was then allowed to stir at rt overnight. The solvent was then removed under reduced pressure, and the solid crude product was washed with acetone (3 × 20 mL). This crude was then dissolved in deionized water to be stirred with 500 mg of Chelex 100, sodium form at rt for 2 h. The reaction solution was then loaded directly onto a C18 reversed-phase column (2 g), and the column was eluted with deionized water (20 mL). The water elution was lyophilized to yield **2** as a white solid (11 mg, 61%): ^{1}H NMR (300 MHz, D_2O) δ 7.71−7.52 (m, 7H), 7.37 (t, J = 6 Hz, 2H), 4.24−4.18 (m, 3H), 3.88−3.63 (m, 10H), 3.03−2.97 (m, 4H), 2.79 (t, J = 6 Hz, 2H), 2.10−2.05 (t, J = 6 Hz, 2H), 1.67−1.68 (m, 1H), 1.46−1.34 (m, 10H), 1.22−1.16 (m, 9H); ^{31}P NMR (121.5 MHz, D_2O) δ 1.33, 1.02, 0.40, −0.89; MALDI-HRMS calcd for $[M + Na]^+$ 1095.2178, found 1095.2285.

*Benzophenone-Lys(alkyne)-hexyl-PI(3,4,5)P_3 (**3**).* Compound **9a** (80 mg, 0.129 mmol) was dissolved in 2 mL of methanol. To this solution was added 2 mL of a 2 M sodium hydroxide aqueous solution. The reaction mixture was stirred at rt overnight and was then added to proton resin to adjust the pH to ~4, followed by removal of the resin by filtration. The filtrate was next concentrated to yield crude acid **9b** as a colorless gum (68 mg, 87%). Acid **9b** (68 mg, 0.112 mmol) was next dissolved in 6 mL of tetrahydrofuran. To this stirred solution were added *N*-[3-(dimethylamino)propyl]-*N*′-ethylcarbodiimide hydrochloride (EDCI, 43 mg, 0.224 mmol) and then *N*-hydroxysuccinimide (26 mg, 0.224 mmol), and the reaction mixture was stirred for 8 h and then concentrated. The crude was next dissolved in 30 mL of chloroform and washed with water (3 × 20 mL). The organic layer was concentrated, and 30 mL of ethyl ether was added, after which the resulting white precipitate was filtered and redissolved in chloroform (15 mL). The solution was then filtered, and the filtrate was concentrated to yield the crude NHS ester corresponding to **9b** as a colorless oil. The crude NHS ester was then dissolved in 1 mL of *N*,*N*-dimethylformamide. To this solution was added **4b**[36] (8 mg, 0.0106 mmol) in 1 mL of tetraethylammonium bicarbonate (TEAB, 1 M, pH 7.5). Additionally, 1 mL of tetrahydrofuran was added to enhance solubility. The reaction mixture was next allowed to stir at rt overnight, at which point the solvent was removed under reduced pressure. The solid crude product was washed with acetone (3 × 20 mL) and then dissolved in deionized water to be stirred with 500 mg of Chelex 100, sodium form at rt for 2 h. The reaction solution was directly loaded onto a C18 reversed-phase column (2 g), and the column was eluted with deionized water (20 mL). The water elution was lyophilized to yield **3** as a white solid (11.2 mg, 93%): ^{1}H NMR (500 MHz, D_2O) δ 7.86−7.80 (m, 4H), 7.76−7.74 (m, 2H), 7.67 (t, J = 3 Hz, 1H), 7.53−7.50 (m, 2H), 4.36−4.33 (m, 3H), 4.03−4.02 (m, 1H), 3.96−3.95 (m, 2H), 3.83−3.79 (m, 3H), 3.16−3.02 (m, 5H), 3.02−2.78 (m, 2H), 2.35−2.31 (m, 4H), 2.09−2.06 (m, 2H), 1.80−1.78 (m, 2H), 1.51−1.18 (m, 18H); ^{31}P NMR (202.5 MHz, D_2O) δ 0.70, 0.31, −0.28, −0.90; MALDI-HRMS calcd for $[M + Na]^+$ 1208.3024, found 1208.2186.

Protein and Cell Extract Labeling Studies. *General Procedure for Protein Labeling.* In a transparent 96-well plate, Akt-PH (50 μL, to a final concentration of 60 μg/mL in PBS) or cytosolic cell extracts [50 μL used in samples for probe **1**, 43 μL used in samples for probes **2** and **3**, of 1.0 mg/mL in PBS buffer (pH 7.4)] were incubated with PIP_n probe **1**, **2**, or **3** (1−200 μM) or bifunctional tag **8a** (50 μM in DMSO) for 1 h at rt. The 96-well plate was then placed on ice and photolyzed for 1 h via placement ~1 cm below a 350 nm Spectroline ENF260C UV lamp. Samples using probe **2** or **3** were followed by derivatization via click chemistry, while samples of probe **1** were directly subjected to sodium dodecyl sulfate−polyacrylamide gel electrophoresis (SDS−PAGE).

*Procedure for Click Reaction using Azido-Rhodamine **11** (probe **2** and **3** only).*[37,42] Following the photolysis procedure, to each sample were added 1 μL rhodamine-N_3 (**11**) (in DMSO to a final concentration of 1 mM), 3 μL tris(2-carboxyethyl)phosphine (TCEP in water to a final concentration of 1 mM), 3 μL ligand [TBTA or THPTA (**18**), in a 1:4 (v/v) DMSO/*tert*-butanol mixture to a final concentration of 100 μM], and 1 μL copper sulfate pentahydrate (50× stock in water to a final concentration of 1 mM). The final volume of each reaction was 50 μL. Samples were shaken for 10 s after each addition. After all additions, samples were incubated at rt for 1 h. For gel analysis, each reaction was quenched by addition of 50 μL of SDS−PAGE sample buffer (2×).

The proteins (30 μL of quenched sample per gel lane) were separated by one-dimensional (1D) SDS−PAGE and visualized via in gel using a fluorescence scanner.

Procedure for Competition Studies with Akt-PH. Akt-PH protein in PBS buffer (pH 7.4, 60 μg/mL) was added into four separate wells of a 96-well microplate (42 μL each). Samples were then incubated with either 0, 2, 5, or 10 mM amino-tagged PI(3,4,5)P_3 (**4b**) (50× stock in water) at 4 °C overnight, prior to incubation with 50 μM probe **2** (2.5 mM stock in water) for 1 h at rt. The final volume of each reaction was 50 μL. The 96-well plate was then placed on ice and photolyzed for 1 h under a 350 nm UV lamp. Next, the click reaction procedure with azido-rhodamine **11** was performed with each sample, followed by SDS−PAGE and fluorescence scanning.

Mass Spectrometry Proteomic Analysis. *Procedure for Sample Preparation.* To three separate tubes were added cytosolic MDA-MB-435 cancer cell extract (870 μL each, 1 mg/mL in PBS for samples I and II or 2 mg/mL in PBS for sample III) and 20 μL of alkyne-PI(3,4,5)P_3 probe **2** (5 mM stock solution in water for a final concentration of 100 μM in samples I and II or 1.25 mM stock solution in water for a final concentration of 25 μM in sample III). Finally, for samples I and II, a control sample was generated using the same conditions with bifunctional tag **8a** lacking PIP headgroups; for sample III, a control sample was generated using the same condition but lacking the addition of any probe. These samples were incubated for 1 h, followed by photolysis on ice via 350 nm irradiation for 1 h. Next, 6 μL of biotin-azide **12** (50 mM in DMSO for a final concentration of 300 μM) was added, followed by 20 μL of tris(2-carboxyethyl)phosphine (TCEP, 50 mM in water for a final concentration of 1 mM), 66 μL of TBTA ligand (1.67 mM in a 1:4 DMSO/*tert*-butanol mixture for a final concentration of 100 μM), and 20 μL of copper sulfate pentahydrate (50 mM in water for a final concentration of 1 mM). These mixtures were incubated at rt for 1 h. Next, to each sample were added 4 mL of methanol, 1 mL of chloroform, and 3 mL of water, and the samples were vortexed and then centrifuged (4000 rpm for 10 min) to pellet proteins. The protein pellet was redissolved in 600 μL of methanol, and 150 μL of chloroform and 600 μL of water were added, after which the samples were vortexed and centrifuged (14000 rpm for 3 min) to pellet the proteins a second time. The protein pellet was then washed with methanol (2 × 600 μL), followed by resuspension in 500 μL of a 6 M urea/25 mM ammonium bicarbonate mixture. Water (500 μL) was added to each sample, each of which was then heated to 65 °C for 5 min. After addition of 50 μL of TCEP (0.1 M for a final concentration of 10 mM), the sample incubation was continued at 65 °C for 15 min. After the samples had been cooled to rt, 40 μL of iodoacetamide (0.55 M in 50 mM ammonium bicarbonate for a final iodoacetamide concentration of 40 mM) was added to each sample and the resulting solutions were incubated at 37 °C for 30 min in the dark. Next, 10% SDS was added to achieve a final concentration of 2%. The samples were next heated to 65 °C for 5 min and then diluted into a 0.2% SDS solution with PBS and 50 mM Tris buffer (3:3.5, v/v). The slurry was then washed with PBS (2×). To this slurry was added streptavidin agarose resin (Thermo Scientific), and the resulting samples were incubated at rt for 1 h with rotation. The resin was centrifuged to pellet (4000 rpm for 3 min) and washed with 1% SDS buffer (2 × 8 mL), 6 M urea (2 × 8 mL), and then PBS buffer (2 × 10 mL). Next, in the resin were resuspended 200 μL of a 2 M urea/25 mM ammonium bicarbonate mixture, 2 μL of calcium chloride (100 mM in water for a final concentration of 1 mM), and 4 μg of trypsin (sequence grade, Promega). Samples were incubated at 37 °C overnight and were then centrifuged to separate the resin from the supernatant. The supernatant was collected and acidified using 5% formic acid for LC-MS/MS analysis. The data generated from samples containing the probe were compared with those from the control studies.

Mass Spectrometry and Data Analysis. Digested peptide mixtures were pressure-loaded onto a biphasic (strong cation exchange, reverse-phase) capillary column and analyzed by two-dimensional liquid chromatography (2D-LC) separation in combination with tandem mass spectrometry, as previously described.[43−45] Mass spectrometry was performed using an Agilent 1200-series quaternary pump and a Thermo Scientific LTQ ion trap mass spectrometer. Peptides were eluted in a five-step MudPIT experiment (using 0, 10, 25, 80, and 100% salt bumps of 500 mM aqueous ammonium acetate), and data were collected in data-dependent acquisition mode with dynamic exclusion turned on (90 s, repeat of 1). Specifically, one full MS (MS1) scan (m/z 400−1800) was followed by seven MS_2 scans of the most abundant ions. The MS^2 spectral data were extracted from the raw files using RAW Xtractor (version 1.9.1; publicly available at http://fields.scripps.edu/downloads.php). MS_2 spectra data were searched using the SEQUEST algorithm (version 3.0) against the latest version of the mouse IPI database concatenated with the reversed database for assessment of false-discovery rates. In total, the search database contained 553 protein sequence entries (549 real sequences and four decoy sequences). SEQUEST searches allowed for variable oxidation of methionine (+16.0), static modification of cysteine residues (+57.0 due to alkylation), no enzyme specificity, and a mass tolerance set to ±1.5 Da for precursor masses and ±0.5 Da for product ion masses. The resulting MS^2 spectra matches were assembled and filtered using DTASelect (version 2.0.47). The validity of peptide−spectrum matches was assessed using DTASelect and two SEQUEST-defined parameters, the cross-correlation score (XCorr) and the normalized difference in cross-correlation scores (DeltaCN). The search results were grouped by charge state (+1, +2, and +3), tryptic status, and modification status (modified and unmodified peptides), resulting in 18 distinct subgroups. In each of these subgroups, the distribution of Xcorr and DeltaCN values for the direct and decoy database hits was obtained, and then the direct and decoy subsets were separated by discriminant analysis. Outlier points in the two distributions were discarded. Full separation of the direct and decoy subsets is not generally possible, so the discriminant score was set such that a false discovery rate of <0.73% was determined on the basis of the number of accepted decoy database peptides. In addition, a minimal peptide length of seven amino acid residues was imposed, and protein identification required the matching of at least two peptides per protein. Such criteria resulted in the elimination of most decoy database hits. Lists of prospective PI(3,4,5)P_3-binding proteins were generated by setting criteria as ≥5-fold (Table 1) or ≥2-fold (Table 2) higher spectral counts in samples containing probe **2** compared to the corresponding negative control sample. Three protein lists were generated from separate runs, and all proteins listed in Table 1 or 2 were detected in at least two of the three runs. Protein functions and domains were determined by searching two databases (http://www.uniprot.org/uniprot and http://pir.georgetown.edu).

Table 1. Proteins Identified in Proteomic Studies with >5-fold Enrichments of Spectral Counts in Probe-Labeled Samples Relative to Controls[a]

accession number	abbreviation	protein
P62191	PRS4	26S protease regulatory subunit 4
Q9BWD1	THIC	acetyl-CoA acetyltransferase, cytosolic
Q99798	ACON	aconitate hydratase, mitochondrial
P61160	ARP2	actin-related protein 2
P54819	KAD2	adenylate kinase 2, mitochondrial
P00568	KAD1	adenylate kinase isoenzyme 1
P15121	ALDR	aldose reductase
P12814	ACTN1	α-actinin-1
O43707	ACTN4	α-actinin-4[25]
P04083	ANXA1	annexin A1
P07355	ANXA2	annexin A2[25]
P14868	SYDC	aspartyl-tRNA synthetase, cytoplasmic
P25705	ATPA	ATP synthase subunit α, mitochondrial
P06576	ATPB	ATP synthase subunit β, mitochondrial
P61221	ABCE1	ATP-binding cassette subfamily E member 1
P53396	ACLY	ATP-citrate synthase
P31939	PUR9	bifunctional purine biosynthesis protein PURH
P11586	C1TC	C-1-tetrahydrofolate synthase, cytoplasmic
P16152	CBR1	carbonyl reductase (NADPH) 1 OS = *Homo sapiens* GN = CBR1 PE = 1 SV = 3
O75828	CBR3	carbonyl reductase (NADPH) 3
P68400	CSK21	casein kinase II subunit α
P19784	CSK22	casein kinase II subunit α′
Q00610	CLH1	clathrin heavy chain 1[25]
P53621	COPA	coatomer subunit α[25]
P21399	ACOC	cytoplasmic aconitate hydratase
Q14204	DYHC1	cytoplasmic dynein 1 heavy chain 1
P09417	DHPR	dihydropteridine reductase
O00429	DNM1L	dynamin-1-like protein
P30084	ECHM	enoyl-CoA hydratase, mitochondrial
Q14240	IF4A2	eukaryotic initiation factor 4A-II
P56537	IF6	eukaryotic translation initiation factor 6
P55060	XPO2	exportin-2[25]
P49327	FAS	fatty acid synthase[25]
P21333	FLNA	filamin-A[25]
P04075	ALDOA	fructose-bisphosphate aldolase A
P17931	LEG3	galectin-3[25]
Q92820	GGH	γ-glutamyl hydrolase
Q06210	GFPT1	glucosamine−fructose-6-phosphate aminotransferase (isomerizing) 1
P11413	G6PD	glucose-6-phosphate 1-dehydrogenase[25]
P06744	G6PI	glucose-6-phosphate isomerase
P04406	G3P	glyceraldehyde-3-phosphate dehydrogenase[25]
P06737	PYGL	glycogen phosphorylase, liver form
P49915	GUAA	GMP synthase (glutamine-hydrolyzing)
P62826	RAN	GTP-binding nuclear protein Ran
Q9NRV9	HEBP1	heme-binding protein 1
P12268	IMDH2	inosine-5′-monophosphate dehydrogenase 2
P02533	K1C14	heratin, type I cytoskeletal 14
P08779	K1C16	keratin, type I cytoskeletal 16
P35527	K1C9	keratin, type I cytoskeletal 9
Q9HA64	KT3K	ketosamine-3-kinase
P33176	KINH	kinesin-1 heavy chain[25]
Q04760	LGUL	lactoylglutathione lyase
P42704	LPPRC	leucine-rich PPR motif-containing protein, mitochondrial[25]
Q93052	LPP	lipoma-preferred partner
P40926	MDHM	malate dehydrogenase, mitochondrial
O95983	MBD3	methyl-CpG-binding domain protein 3
P26038	MOES	moesin[25]
P35579	MYH9	myosin-9[25]
P43490	NAMPT	nicotinamide phosphoribosyltransferase
P06748	NPM	nucleophosmin[25]
P15531	NDKA	nucleoside diphosphate kinase A
P30041	PRDX6	peroxiredoxin-6
P30086	PEBP1	phosphatidylethanolamine-binding protein 1
P00558	PGK1	phosphoglycerate kinase 1
Q9Y617	SERC	phosphoserine aminotransferase
Q15365	PCBP1	poly(rC)-binding protein 1
P26599	PTBP1	polypyrimidine tract-binding protein 1
O60568	PLOD3	procollagen-lysine, 2-oxoglutarate 5-dioxygenase
P48147	PPCE	prolyl endopeptidase
Q9UL46	PSME2	proteasome activator complex subunit 2
P61289	PSME3	proteasome activator complex subunit 3
P28070	PSB4	proteasome subunit β type 4
Q99497	PARK7	protein DJ-1
Q92597	NDRG1	protein NDRG1
P31150	GDIA	Rab GDP dissociation inhibitor α
P35241	RADI	radixin
P46940	IQGA1	Ras GTPase-activating-like protein IQGAP1[25]
Q15019	SEP3	septin-2[25]
P34897	GLYM	serine hydroxymethyltransferase, mitochondrial
P30153	2AAA	serine/threonine-protein phosphatase 2A 65 kDa regulatory subunit A α isoform
P02768	ALBU	serum albumin
Q13813	SPTA2	spectrin α chain, brain[25]
P17987	TCPA	T-complex protein 1 subunit α
P50991	TCPD	T-complex protein 1 subunit δ
Q99832	TCPH	T-complex protein 1 subunit η
P50990	TCPQ	T-complex protein 1 subunit θ
P40227	TCPZ	T-complex protein 1 subunit ζ
Q8NBS9	TXND5	thioredoxin domain-containing protein 5
P23193	TCEA1	transcription elongation factor A protein 1
Q92616	GCN1L	translational activator GCN1[25]
P23381	SYWC	tryptophanyl-tRNA synthetase, cytoplasmic
P30085	KCY	UMP-CMP kinase
Q16831	UPP1	uridine phosphorylase 1
P38606	VATA	V-type proton ATPase catalytic subunit A
P21281	VATB2	V-type proton ATPase subunit B, brain isoform
P49748	ACADV	very long-chain specific acyl-CoA dehydrogenase, mitochondrial[25]
P13010	XRCC5	X-ray repair cross-complementing protein 5

[a]References are included for those proteins that have been identified in other global proteomic studies.

RESULTS

Design and Synthesis of PIP$_n$ Headgroup Activity-Based Probes. Activity-based probes generally consist of analogues of the natural substrate or ligand of interest in which two groups are introduced: (1) a reactive functional group that allows for the covalent labeling of target proteins and (2) a secondary tag that allows selective detection and/or purification of proteins that have been successfully labeled by the probe. Activity probes corresponding to ligands that interact with proteins solely through noncovalent binding interactions typically employ photoaffinity tags[46] to enforce covalent labeling of target proteins.[33,34,47−50] For this purpose, we implemented the benzophenone group because of its robust

Table 2. Proteins Identified via Proteomic Studies with 2−5-fold Enrichments of Spectral Counts in Probe-Labeled Samples Relative to Controls[a]

accession number	abbreviation	protein
P61604	CH10	10 kDa heat shock protein, mitochondrial
P31946	1433B	14-3-3 protein β/α
Q04917	1433F	14-3-3 protein η
P61981	1433G	14-3-3 protein γ
P43686	PRS6B	26S protease regulatory subunit 6B
P62195	PRS8	26S protease regulatory subunit 8
Q99460	PSMD1	26S proteasome non-ATPase regulatory subunit 1
Q6NVY1	HIBCH	3-hydroxyisobutyryl-CoA hydrolase, mitochondrial
P62841	RS15	40S ribosomal protein S15
P08708	RS17	40S ribosomal protein S17
P15880	RS2	40S ribosomal protein S2
P23396	RS3	40S ribosomal protein S3
P61247	RS3A	40S ribosomal protein S3a
P62081	RS7	40S ribosomal protein S7
P46781	RS9	40S ribosomal protein S9
Q5TFE4	NT5D1	5′-nucleotidase domain-containing protein 1
P17858	K6PL	6-phosphofructokinase, liver type[25]
P08237	K6PF	6-phosphofructokinase, muscle type
P10809	CH60	60 kDa heat shock protein, mitochondrial
P46778	RL21	60S ribosomal protein L21
P62750	RL23A	60S ribosomal protein L23a
P36578	RL4	60S ribosomal protein L4
P46777	RL5	60S ribosomal protein L5
P62424	RL7A	60S ribosomal protein L7a
P11021	GRP78	78 kDa glucose-regulated protein
P24752	THIL	acetyl-CoA acetyltransferase, mitochondrial
O15144	ARPC2	actin-related protein 2/3 complex subunit 2
O15145	ARPC3	actin-related protein 2/3 complex subunit 3
P55263	ADK	adenosine kinase
P49588	SYAC	alanyl-tRNA synthetase, cytoplasmic
P61163	ACTZ	α-centractin
P08133	ANXA6	annexin A6
Q9BZZ5	API5	apoptosis inhibitor 5
Q96P48	ARAP1	Arf-GAP with Rho-GAP domain, ANK repeat and PH domain-containing protein 1[30]
P54136	SYRC	arginyl-tRNA synthetase, cytoplasmic
P08243	ASNS	asparagine synthetase (glutamine-hydrolyzing)
Q13057	COASY	bifunctional coenzyme A synthase
P27797	CALR	calreticulin
O43852	CALU	calumenin
O00299	CLIC1	chloride intracellular channel protein 1[25]
Q9Y696	CLIC4	chloride intracellular channel protein 4
Q00610	CLH1	clathrin heavy chain 1[25]
P53621	COPA	coatomer subunit α[25]
Q07021	C1QBP	complement component 1 Q subcomponent-binding protein, mitochondrial
P04080	CYTB	cystatin-B
Q9UHD1	CHRD1	cysteine- and histidine-rich domain-containing protein 1
P28838	AMPL	cytosol aminopeptidase
O00154	BACH	cytosolic acyl-coenzyme A thioester hydrolase
Q96KP4	CNDP2	cytosolic nonspecific dipeptidase
P54886	P5CS	Δ-1-pyrroline-5-carboxylate synthase
P15924	DESP	desmoplakin
Q16555	DPYL2	dihydropyrimidinase-related protein 2
P28340	DPOD1	DNA polymerase δ catalytic subunit
P49736	MCM2	DNA replication licensing factor MCM2
P31689	DNJA1	DnaJ homologue subfamily A member 1
Q9H223	EHD4	EH domain-containing protein[25]
P13804	ETFA	electron transfer flavoprotein subunit α, mitochondrial
P13639	EF2	elongation factor 2
P49411	EFTU	elongation factor Tu, mitochondrial
P60842	IF4A1	eukaryotic initiation factor 4A-I
P62495	ERF1	eukaryotic peptide chain release factor subunit 1
P60228	EIF3E	eukaryotic translation initiation factor 3 subunit E
Q15056	IF4H	eukaryotic translation initiation factor 4H
P63241	IF5A1	eukaryotic translation initiation factor 5A-1
P49327	FAS	fatty acid synthase[25]
O75369	FLNB	filamin-B[25]
P39748	FEN1	flap endonuclease 1
P07954	FUMH	fumarate hydratase, mitochondrial
P17931	LEG3	galectin-3[25]
Q13630	FCL	GDP-L-fucose synthase
P06396	GELS	gelsolin[24]
O94925	GLSK	glutaminase kidney isoform, mitochondrial
Q9Y2Q3	GSTK1	glutathione *S*-transferase κ 1
P21266	GSTM3	glutathione *S*-transferase μ 3
P04406	G3P	glyceraldehyde-3-phosphate dehydrogenase[25]
P11216	PYGB	glycogen phosphorylase, brain form
P08238	HS90B	heat shock protein HSP 90-β
Q14103	HNRPD	heterogeneous nuclear ribonucleoprotein D0
P52597	HNRPF	heterogeneous nuclear ribonucleoprotein F
P61978	HNRPK	heterogeneous nuclear ribonucleoprotein K
P26583	HMGB2	high-mobility group protein B2
Q16836	HCDH	hydroxyacyl-coenzyme A dehydrogenase, mitochondrial
Q9UI26	IPO11	importin-11
P50213	IDH3A	isocitrate dehydrogenase (NAD) subunit α, mitochondrial
P26440	IVD	isovaleryl-CoA dehydrogenase, mitochondrial
P14923	PLAK	junction plakoglobin
P08779	K1C16	keratin, type I cytoskeletal 16
P35527	K1C9	keratin, type I cytoskeletal 9
P04264	K2C1	keratin, type II cytoskeletal 1
P35908	K22E	keratin, type II cytoskeletal 2 epidermal
P33176	KINH	kinesin-1 heavy chain[25]
P07195	LDHB	L-lactate dehydrogenase B chain
Q32MZ4	LRRF1	leucine-rich repeat flightless-interacting protein 1
Q8N1G4	LRC47	leucine-rich repeat-containing protein 47
O60711	LPXN	leupaxin
P40925	MDHC	malate dehydrogenase, cytoplasmic
Q9UNF1	MAGD2	melanoma-associated antigen D2
Q15691	MARE1	microtubule-associated protein RP/EB family member 1[25]
P28482	MK01	mitogen-activated protein kinase 1[25]
P60660	MYL6	myosin light polypeptide 6[25]
O00159	MYO1C	myosin-Ic
P51606	RENBP	*N*-acylglucosamine 2-epimerase
Q14697	GANAB	neutral α-glucosidase AB
Q15233	NONO	non-POU domain-containing octamer-binding protein
Q8TAT6	NPL4	nuclear protein localization protein 4 homologue
P12270	TPR	nucleoprotein TPR
Q8WXF1	PSPC1	paraspeckle component 1
P62937	PPIA	peptidyl-prolyl cis−trans isomerase A
Q13526	PIN1	peptidyl-prolyl cis−trans isomerase NIMA-interacting 1
Q13162	PRDX4	peroxiredoxin-4[30]

dx.doi.org/10.1021/bi201636s | *Biochemistry* 2011, 50, 11143−11161

Table 2. continued

accession number	abbreviation	protein
Q9Y2H2	SAC2	phosphatidylinositide phosphatase SAC2
Q13492	PICAL	phosphatidylinositol-binding clathrin assembly protein[24]
Q15149	PLEC	plectin
Q6P2Q9	PRP8	pre-mRNA-processing splicing factor 8
Q99471	PFD5	prefoldin subunit 5
P02545	LMNA	prelamin-A/C
P26196	DDX6	probable ATP-dependent RNA helicase DDX6
P28066	PSA5	proteasome subunit α type 5
P20618	PSB1	proteasome subunit β type 1
P49720	PSB3	proteasome subunit β type 3
P28072	PSB6	proteasome subunit β type 6
Q99436	PSB7	proteasome subunit β type 7
P28062	PSB8	proteasome subunit β type 8
P28065	PSB9	proteasome subunit β type 9
P30101	PDIA3	protein disulfide isomerase A3
P07237	PDIA1	protein disulfide isomerase
Q9NUQ9	FA49B	protein FAM49B
P22061	PIMT	protein-L-isoaspartate(D-aspartate) *O*-methyltransferase
Q9NVS9	PNPO	pyridoxine-5′-phosphate oxidase
P50395	GDIB	Rab GDP dissociation inhibitor β
P31153	METK2	*S*-adenosylmethionine synthase isoform type 2
P10768	ESTD	*S*-formylglutathione hydrolase
Q16181	SEP3	septin-7[25]
Q9UHD8	SEP10	septin-9[25]
Q13501	SQSTM	sequestosome-1
P63151	2ABA	serine/threonine-protein phosphatase 2A 55 kDa regulatory subunit B α isoform[25]
Q15257	PTPA	serine/threonine-protein phosphatase 2A activator
P62136	PP1A	serine/threonine-protein phosphatase PP1-α catalytic subunit[25]
P50454	SERPH	serpin H1[30]
Q01082	SPTB2	spectrin β chain, brain 1[25]
Q15637	SF01	splicing factor 1
Q13435	SF3B2	splicing factor 3B subunit 2
Q15393	SF3B3	splicing factor 3B subunit 3
P26368	U2AF2	splicing factor U2AF 65 kDa subunit
P31948	STIP1	stress-induced phosphoprotein 1
Q9UH65	SWP70	switch-associated protein 70[30]
Q99536	VAT1	synaptic vesicle membrane protein VAT-1 homologue
P78371	TCPB	T-complex protein 1 subunit β
P48643	TCPE	T-complex protein 1 subunit ε
P49368	TCPG	T-complex protein 1 subunit γ
O95881	TXD12	thioredoxin domain-containing protein 12
Q15645	TRP13	thyroid receptor-interacting protein 13
P20290	BTF3	transcription factor BTF3
Q8WXI9	P66B	transcriptional repressor p66-β
Q9Y5L0	TNPO3	transportin-3
P22102	PUR2	trifunctional purine biosynthetic protein adenosine-3
P60174	TPIS	triosephosphate isomerase
P23381	SYWC	tryptophanyl-tRNA synthetase, cytoplasmic
P07437	TBB5	tubulin β chain
P04350	TBB4	tubulin β-4 chain
Q6IBS0	TWF2	twinfilin-2
O15042	SR140	U2-associated protein SR140
Q93009	UBP7	ubiquitin carboxyl-terminal hydrolase 7
P61088	UBE2N	ubiquitin-conjugating enzyme E2 N[25]
Q04323	UBXN1	UBX domain-containing protein 1
P54727	RD23B	UV excision repair protein RAD23 homologue B
P50552	VASP	vasodilator-stimulated phosphoprotein
Q9NQW7	XPP1	Xaa-Pro aminopeptidase 1

[a]References are included for those proteins that have been identified in other global proteomic studies.

nature and ease of synthesis. On the basis of these principles, our designs for activity probes (**1**−**3**) based on PIP_n headgroups are shown in Figure 1.

The probes illustrated in Figure 1 contain different secondary tags, including a fluorescein moiety (**1**) for direct in-gel detection of probe-labeled products or alkynes (**2** and **3**) as latent bioorthogonal[51,52] reactive groups. The alkynes in the latter probes were employed for selective derivatization after protein labeling via click chemistry to introduce rhodamine for in-gel detection or biotin for affinity purification. This approach has proven to be successful for avoiding disadvantages that can result from initial attachment of bulky reporter tags.[42] To introduce the two tags into each structure, we exploited lysine as a Y-shaped linker, with the benzophenone introduced at the α-amino group and the secondary tag appended to the side chain. Probe **3** included a longer linker between the PIP_n headgroup and the photoaffinity tag because it is known that this distance affects the magnitude of protein cross-linking. Finally, probes corresponding to both $PI(3,4)P_2$ (**1**) and $PI(3,4,5)P_3$ (**2**,**3**) were developed and studied.

In structures **1**−**3**, the ligand motif consists of the PIP_n headgroup linked via the traditional phosphodiester at position 1 to a shortened hexyl linker attached to the reporter groups. Here, the glycerolipid backbone of the PIP_ns is excluded to present the photoaffinity tag closer to bound protein targets to promote labeling. Indeed, the proximity of the benzophenone was found to be important for successful protein labeling (see Discussion). While the short hexyl chain provides hydrophobic character to mimic that of the glycerolipid backbone, these simplified headgroup compounds benefit from water solubility. This circumvents the potential concern that the photoaffinity tag may be buried in the membrane core if full phospholipid analogues were used. In addition, hydrophilic probes were expected to be beneficial for avoiding nonspecific protein binding that often results from hydrophobic interactions. Finally, it is known that many proteins bind simplified soluble PIP_n headgroups with high affinity outside of the membrane environment,[53−57] which is particularly the case with heavily phosphorylated isomers such as $PI(3,4,5)P_3$. For each of these reasons, we elected to utilize simplified headgroup probes bearing short hydrophobic moieties.

The synthesis of the described activity probes benefited from significant advances in PIP_n synthetic strategies in recent years.[1,58−61] We exploited the strategy of using amino conjugates[62−70] of PIP_n headgroups as modular intermediates that can be efficiently derivatized to produce a range of probes through amide bond formation. For this purpose, we recently described the synthesis of aminohexyl headgroup analogues of type **4** (Scheme 1) corresponding to all seven naturally occurring PIP_n isomers.[36] Using this strategy, probes **1**−**3** were each synthesized in one step from the appropriate PIP_n

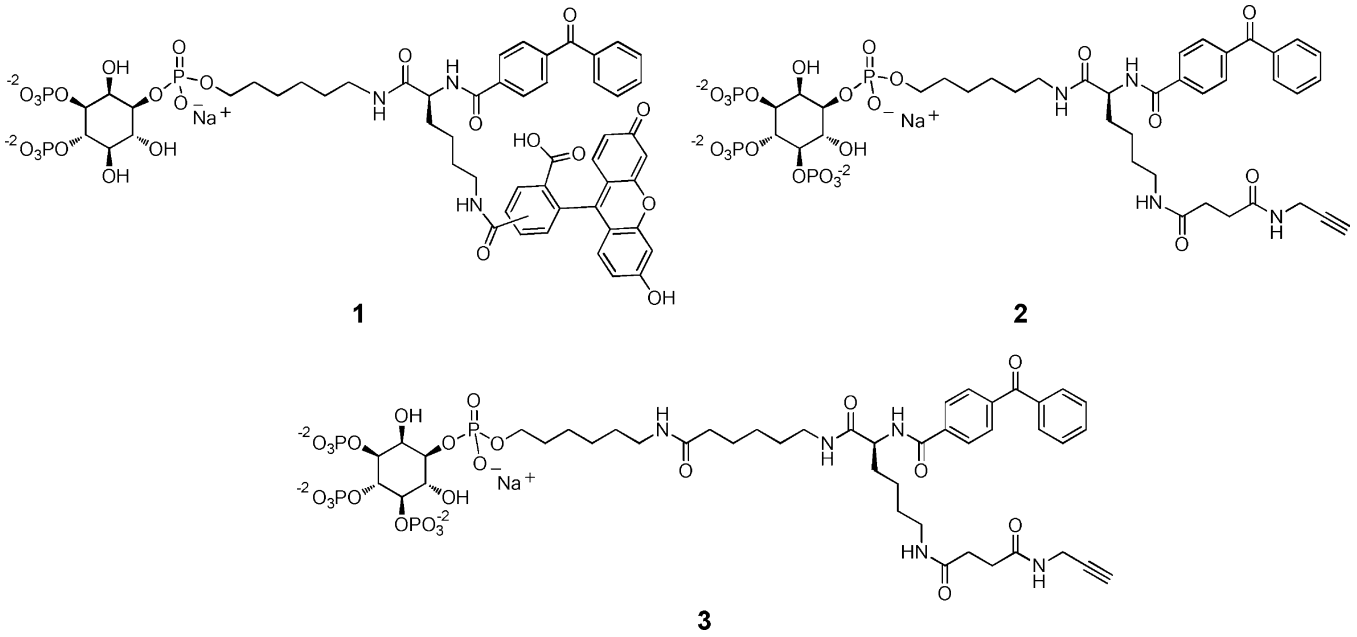

Figure 1. Design of bifunctional PIP_n activity-based probes. Probes consist of the binding moiety (PIP_n headgroup), linked to a Y-shaped lysine linker containing both a photoaffinity group (benzophenone) and a secondary tag that consisted of either fluorescein (probe **1**) or an alkyne as a bioorthogonal tag (probes **2** and **3**).

Scheme 1. General Synthetic Route to PIP_n Activity Probes Using Headgroup−Amino Conjugates of Type 4

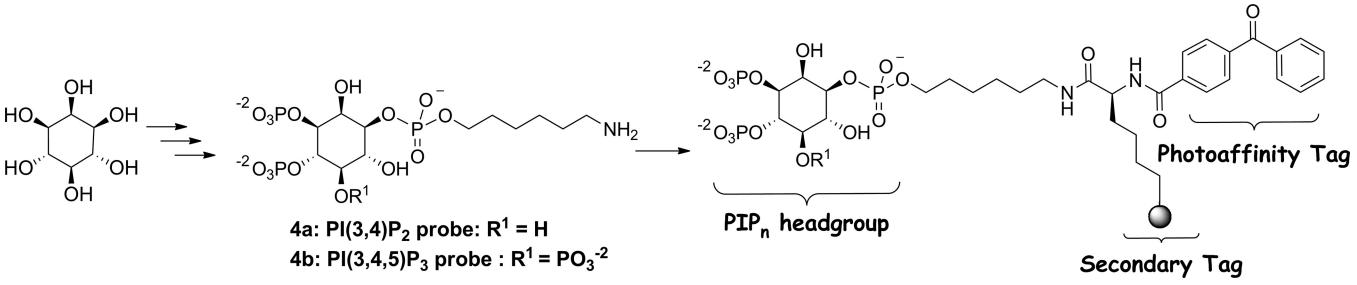

headgroup−amino conjugate, either **4a** to produce $PI(3,4)P_2$ probe **1** or **4b** to generate $PI(3,4,5)P_3$ probes **2** and **3**.

The synthetic routes employed to access the bifunctional lysine handles corresponding to each probe are depicted in Scheme 2. Each of these began with the removal of the carboxybenzyl group (Cbz) of fully protected lysine derivative **5**, followed by coupling of the resulting amino group with 4-benzoylbenzoic acid to introduce the benzophenone photoaffinity tag,[71] and finally Boc deprotection to common intermediate **6**. To produce $PI(3,4)P_2$ probe **1**, compound **6** was coupled to 5(6)-carboxyfluorescein to generate **7a**, followed by ester hydrolysis to carboxylic acid **7b**, which was then converted to the corresponding *N*-hydroxysuccinimidyl (NHS) ester, and finally coupled with amine **4a**. Compounds **2** and **3** were both produced from carboxylic acid **8b**, which was generated through coupling of amine **6** to alkynyl-carboxylic acid **10** to **8a**, followed by ester hydrolysis. Compound **8b** was converted to an NHS ester and coupled to amine **4b** to produce $PI(3,4,5)P_3$ probe **2**. Finally, probe **3** was accessed by coupling **8b** with 6-aminocaproic acid to yield **9a**, followed by ester hydrolysis to **9b**, and conversion to the corresponding NHS ester, which was then coupled with $PI(3,4,5)P_3$ headgroup−amine conjugate **4b**.

Analysis of Protein Labeling by PIP_n Activity Probes Using the PH Domain of Akt as a Purified Protein Target. To obtain an initial assessment of the efficacy of the described activity probes for covalently labeling cognate protein binding partners, we performed studies employing the PH domain of Akt as a known target for both $PI(3,4)P_2$ and $PI(3,4,5)P_3$ (Figure 2).[39,72,73] These initial studies were performed by labeling Akt-PH with probe **1** (lanes 1−3) or **2** (lanes 4 and 5). Labeling experiments were generally performed as follows. Akt-PH was incubated with probe **1** or **2** for 1 h at room temperature, followed by irradiation on ice with 350 nm light for 1 h. Products of experiments involving probe **1** were then directly subjected to 1D SDS−PAGE for in-gel fluorescence analysis due to the presence of fluorescein in the probe. Samples involving probe **2** utilized an intermediate step after photolysis in which click chemistry was exploited to label the alkyne of this probe through reaction with rhodamine-azide **11**, followed by in-gel detection via fluorescence imaging (see Discussion for further details on postlabeling). The results of these experiments showed that Akt-PH was successfully labeled by both $PI(3,4)P_2$-fluorescein probe **1** (lane 2) and $PI(3,4,5)P_3$-alkyne probe **2** (lane 4). Please note that a color version of the fluorescence gel image in Figure 1 is also included as Figure S1 of the Supporting Information.

A potential concern in any cross-linking experiment is that labeling may result from nonspecific interactions of the probe with proteins that are not cognate binding partners. This is

Scheme 2. Synthesis of Bifunctional Lysine Moieties Bearing Different Secondary Tags To Generate PIP$_n$ Activity Probes 1−3[a]

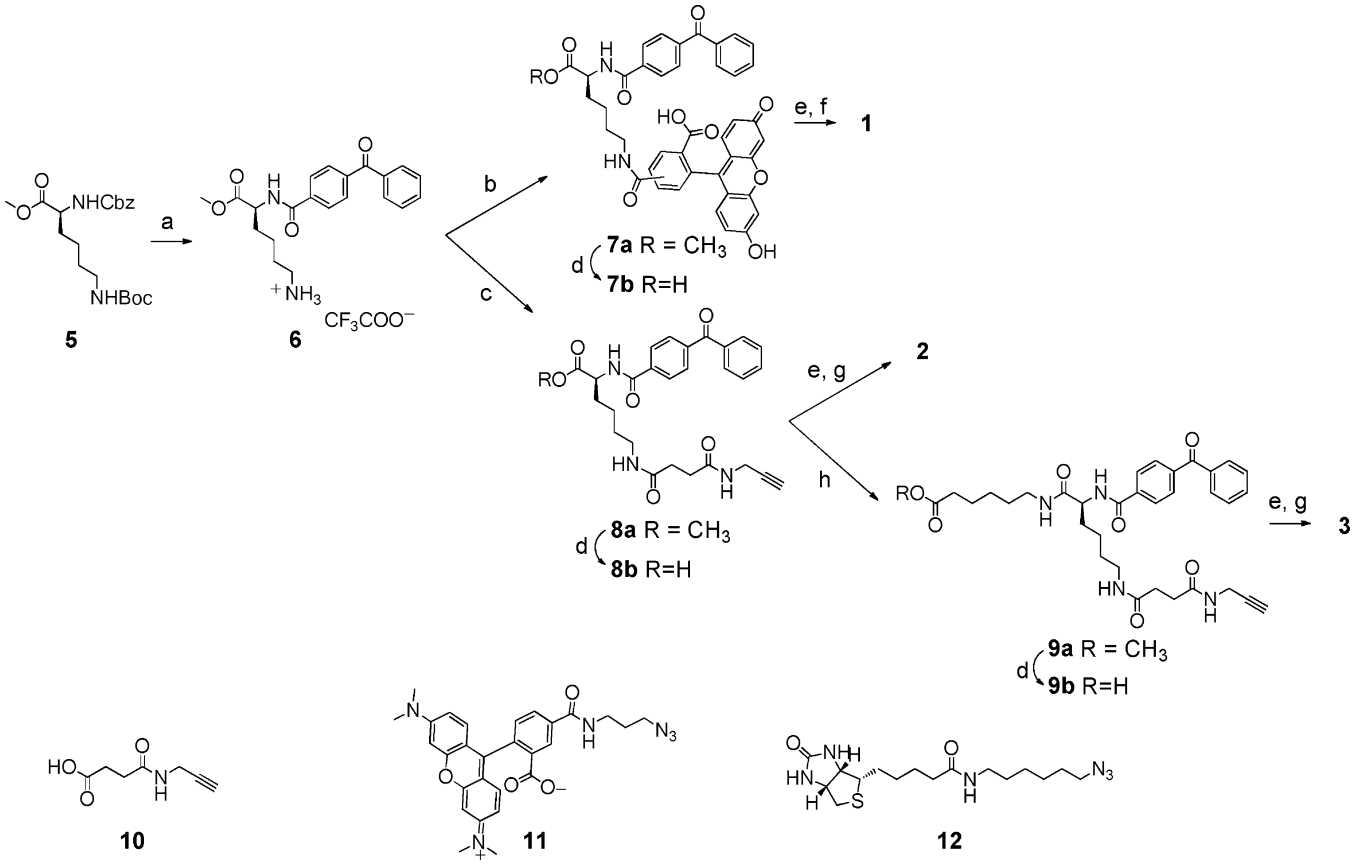

[a](a) (i) H_2, $Pd(OH)_2$, MeOH; (ii) 4-benzoylbenzoic acid, EDCI, NMM, DMAP, DMF; (iii) TFA, CH_2Cl_2; (b) EDCI, NMM, DMAP, DMF, 5(6)-carboxylfluorescein; (c) **10**, EDCI, NMM, DMAP, MeOH/$CHCl_3$; (d) NaOH, MeOH; (e) NHS, DCC, THF; (f) **4a**, TEAB, DMF, THF; (g) **4b**, TEAB, DMF, THF; (h) 6-aminocaproic acid methyl ester hydrochloride, EDCI, NMM, DMAP, MeOH/$CHCl_3$.

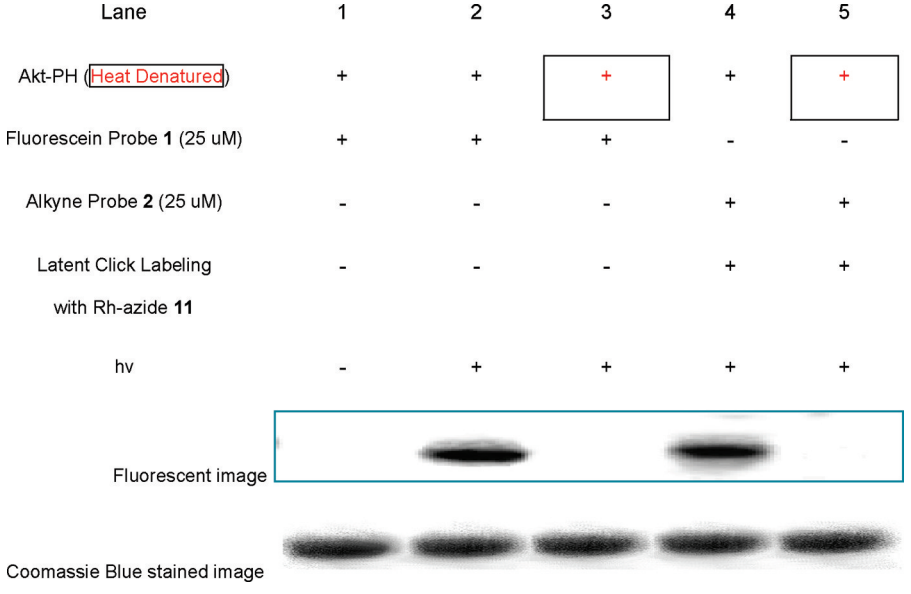

Figure 2. Gel images from labeling studies using purified Akt-PH (fluorescent gel image shown in gray scale). Studies indicated successful labeling of Akt-PH protein by both fluorescein-probe **1** (lane 2) and alkyne-probe **2** (lane 4, after click chemistry postderivatization) during studies. Additionally, control studies involving no photo-cross-linking (lane 1) or heat denaturation of the protein prior to incubation of the probe (lanes 3 and 5) yielded no fluorescence, indicating the absence of nonspecific labeling. Finally, Coomassie Blue stains indicate that the protein is still present despite the abrogation of probe labeling. Please also see the color fluorescence gel scans in Figure S1 of the Supporting Information.

particularly the case with photoaffinity tags, which generate highly reactive intermediates upon photolysis. As such, control experiments are important for demonstrating whether labeling events are driven by specific binding interactions. One control

study we performed to further scrutinize binding involved the initial heat denaturation of the protein target prior to probe incubation, which should abrogate labeling due to the loss of the protein binding domain upon destruction of its higher-order structure. As one can see in Figure 2, for both probe **1** (lane 3) and probe **2** (lane 5), initial heat denaturation of Akt-PH negated protein labeling, which was expected. Probe **1** was subjected to an additional control in which irradiation was not performed (lane 1), which also led to no protein labeling. These results demonstrate that the labeling of Akt-PH involves specific binding and that the photoaffinity tag is critical for on-gel detection of protein labeling.

Further control studies designed to verify that the PIP_n headgroup is responsible for protein labeling involved competition binding using soluble unlabeled $PI(3,4,5)P_3$ headgroup analogue **4b** and probe **2**. As shown in Figure 3,

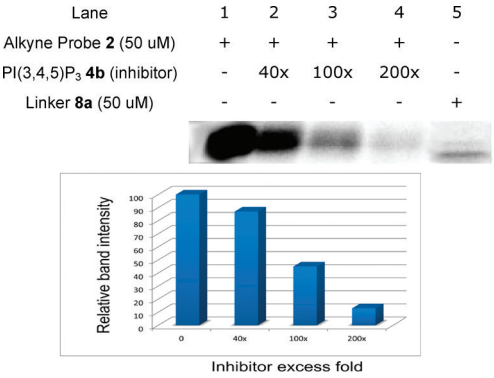

Figure 3. Competition studies involving Akt-PH labeling (fluorescent gel image shown in gray scale). In lanes 1−4, preincubation of Akt-PH with excess inhibitor **4b** suppressed labeling by probe **2** as visualized by a reduction in the fluorescence intensity of the Akt-PH band. In lane 5, the bifunctional lysine lacking the PIP headgroup did not label the Akt protein.

competition was observed with a 40-fold excess of inhibitor **4b** and increased with higher concentrations of this competitor up to a 200-fold excess, which abrogated most of the labeling event (lanes 1−4). Once again, Coomassie Blue stains showed that the protein was still present in each lane (not shown). It is likely that high competitor concentrations are required because probe **2** has a competitive advantage in that it yields irreversible covalent protein labeling, while competitor **4b** acts through reversible noncovalent binding. Finally, to rule out the possibility that the bifunctional lysine tag can label protein on its own, compound **8a** lacking a PIP_n headgroup was also tested for protein labeling (lane 5). Following incubation, cross-linking, and click chemistry with the rhodamine reporter tag, the result showed no labeling of Akt-PH, although it appears that a small impurity in the protein sample just below Akt-PH is labeled in this case. It is possible that **8a** might lead to enhanced nonspecific labeling because of the hydrophobicity of this compound, leading it to insert into hydrophobic pockets on random proteins. Indeed, it is plausible that probes **1** and **2** would avoid nonspecific labeling events, as was observed through the control studies described herein, because of their hydrophilic nature.

It has previously been observed that the nature of the linker between the ligand motif and a photoaffinity tag can affect the efficiency of protein labeling, in some cases leading to dramatic variations.[47,48,74] In particular, differences in linker lengths can cause noticeable discrepancies in protein labeling. To explore how linker length affected the current studies, we compared probes **2** and **3**, the latter containing a longer linker, in terms of the labeling of Akt-PH (Figure 4). Here, we found that probe **3**

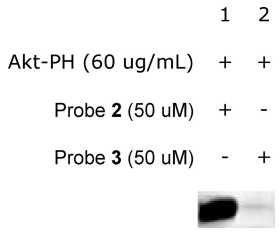

Figure 4. Akt-PH labeling studies with probes **2** and **3** indicate that the shorter linker (probe **2**) results in significantly enhanced protein labeling (fluorescent gel image shown in gray scale).

exhibited virtually no labeling of Akt-PH (lane 2) when compared to probe **2**. Once again, Coomassie Blue stains showed that the protein remains present in each lane (not shown). These results can be rationalized as follows: while the longer linker provides more flexibility for the bifunctional lysine motif, the benzophenone photoaffinity group can react with proteins only in its proximity, and this flexibility may provide too much freedom such that the benzophenone does not spend enough time proximal to the bound protein. These studies again show that the linker between the ligand moiety and photoaffinity tag is critical for effective protein labeling.

Labeling of Proteins in Cell Extracts Using PIP_n Probes. Following initial studies involving the labeling of purified Akt-PH protein, we moved on to more complex studies employing cell extracts. The strategy underlying these experiments is depicted in Figure 5, and probe **2** was generally used for studies because click chemistry allows for postlabeling with different reporter groups and this compound was more effective in protein labeling than probe **3**. First, cell lysates were incubated with the probe to allow for binding of cognate protein binding partners via noncovalent interactions. Next, irradiation with 350 nm light was performed to capture these binding events through covalent cross-linking between the probe and bound proteins. The appropriate tag (rhodamine for in-gel visualization or biotin for affinity purification) was then appended to the protein−probe adducts via click chemistry. We specifically chose cancer cell extracts for studies because of the involvement of PIP_n signaling in tumorigenesis.

We began cell extract labeling experiments by studying a soluble proteome preparation of human melanoma cell line MDA-MB-435 using various concentrations of probe and azido-rhodamine **11**. Experiments were conducted following the protocol outlined in Figure 5 with heat-denatured proteome samples used as controls. The resulting gel showed that a number of fluorescence-labeled protein bands were present (Figure 6). In the heat-denatured controls, certain bands were found to show weakened labeling, particularly in the low mass range. It is also worth mentioning that some of the bands were enriched in heat-denatured samples, particularly in the higher mass range. However, it is often difficult to judge whether these enriched proteins were the same ones that were labeled in the regular sample. Images of Coomassie Blue-stained gels showed identical bands for all lanes (not shown), indicating the presence of the same amount of protein in each sample.

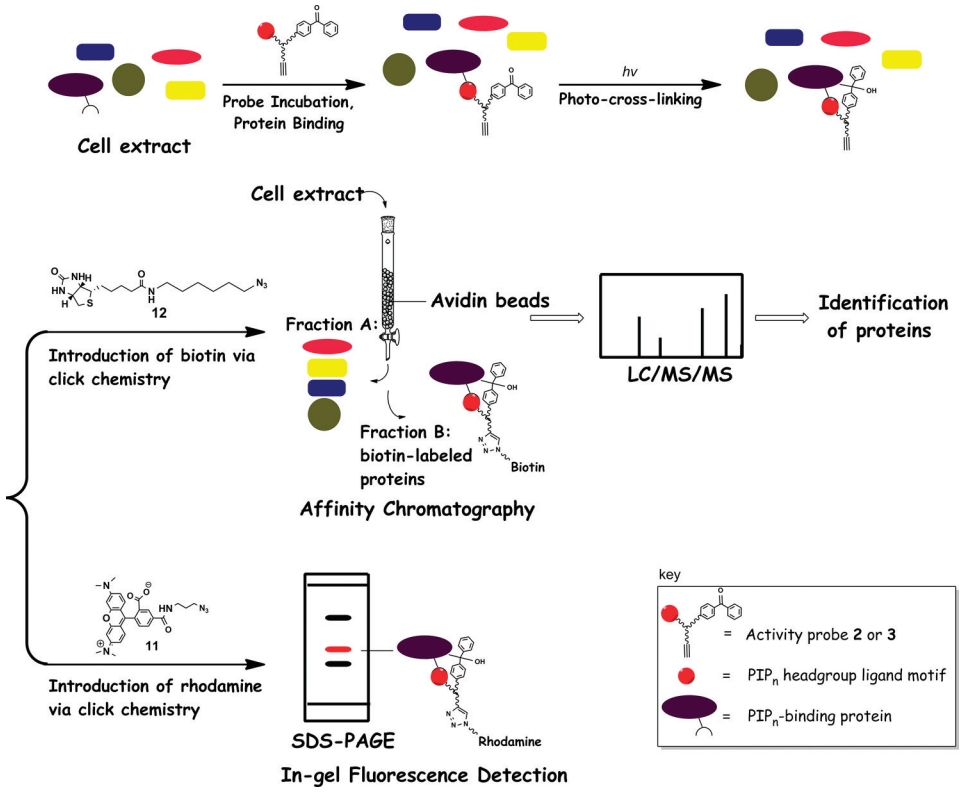

Figure 5. Illustration of the mechanisms of protein labeling and subsequent analysis using alkynyl-PI(3,4,5)P_3 activity probes **2** and **3**. Following the incubation of the probes with cell extracts, protein−probe binding events were captured through irradiation of the benzophenone tag. Next, labeled proteins were selectively derivatized via click chemistry using the secondary functional tag of the probe to introduce rhodamine (**11**) for in-gel fluorescence analysis or biotin (**12**) for protein enrichment via affinity chromatography and subsequent protein identification using liquid chromatography and tandem mass spectrometry.

From these results, a probe concentration of 25 or 50 μM was selected for each of the following labeling studies to optimize the balance between high-intensity labeling and low-intensity background. Please note that a color version of the fluorescence gel image in Figure 6 is also included as Figure S2 of the Supporting Information.

Next, both alkyne-labeled probe **2** and fluorescein-labeled probe **1** were used for labeling studies with the human MDA-MB-435 soluble proteome (Figure 7). Here, studies involving fluorescein-labeled probe **1** (lane 1) clearly resulted in higher levels of background labeling in the heat-denatured control (lane 2) when compared to studies using alkyne probe **2** [lane 4 vs lane 5 (heat-denatured)]. It is likely that the enhancement in the labeling of heat-denatured samples using probe **1** results from nonspecific interactions caused by the presence of the fluorescein moiety during the protein labeling event. In the heat-denatured control, involving probe **2** (lane 5), while a number of bands were observed to be weaker compared to those in the corresponding normal study (lane 4), some enhanced signals likely attributable to nonspecific labeling were again observed in the heat-denatured sample. Further controls, including the absence of probe **2** (lane 6) and a lack of irradiation (lane 8), once again demonstrated that both the probe and photo-cross-linking steps are necessary for protein labeling and in-gel detection. Finally, we analyzed different conditions for postlabeling via click chemistry during studies. It is known that copper-chelating ligands enhance click chemistry reactions, and two different ligand additives were analyzed here. As with previously described experiments, lanes 1−8 utilized the ligand TBTA[75] to enhance the click reaction. We compared these results to those with THPTA [compound **18** (Supporting Information)], a ligand with enhanced water solubility[38,76] (lane 9), and found that the protein labeling results were quite similar using the different ligands. As a result, TBTA was employed in subsequent labeling studies because it is commercially available. Please note that a color version of the fluorescence gel image in Figure 7 is also included as Figure S3 of the Supporting Information.

Next, we analyzed multiple cancer cell proteomes (MDA-MB-435, MDA-MB-231, MCF7, and T47D) to test the general applicability of this strategy. Both the soluble and membrane fractions of each of these cell extracts were tested and compared using both alkyne probe **2** and fluorescein probe **1**, along with heat-denatured proteomes (see fluorescent gel image in Figure S4 of the Supporting Information). Once again, fluorescein probe **1** yielded significantly enhanced labeling in heat-denatured controls, implicating postlabeling as the more effective approach for analysis. The results also demonstrated that the majority of protein labeling occurred with the soluble portion of the proteomes, which is consistent with the fact that many PIP$_n$-binding proteins are soluble peripheral proteins that only interact with the membrane surface upon PIP$_n$ binding. This result is further influenced by the soluble nature of the probes. Finally, it should be noted that probes **1** [PI(3,4)P_2] and **2** [PI(3,4,5)P_3] correspond to different PIP$_n$ headgroup isomers, and thus, it would be expected that they would label a different but overlapping set of proteins.

Using cell extract studies, we once again addressed the issue of the effect of linker length on protein labeling by comparing probes **2** and **3**. As one can see in Figure 8, the results of these

dx.doi.org/10.1021/bi201636s | *Biochemistry* 2011, 50, 11143−11161

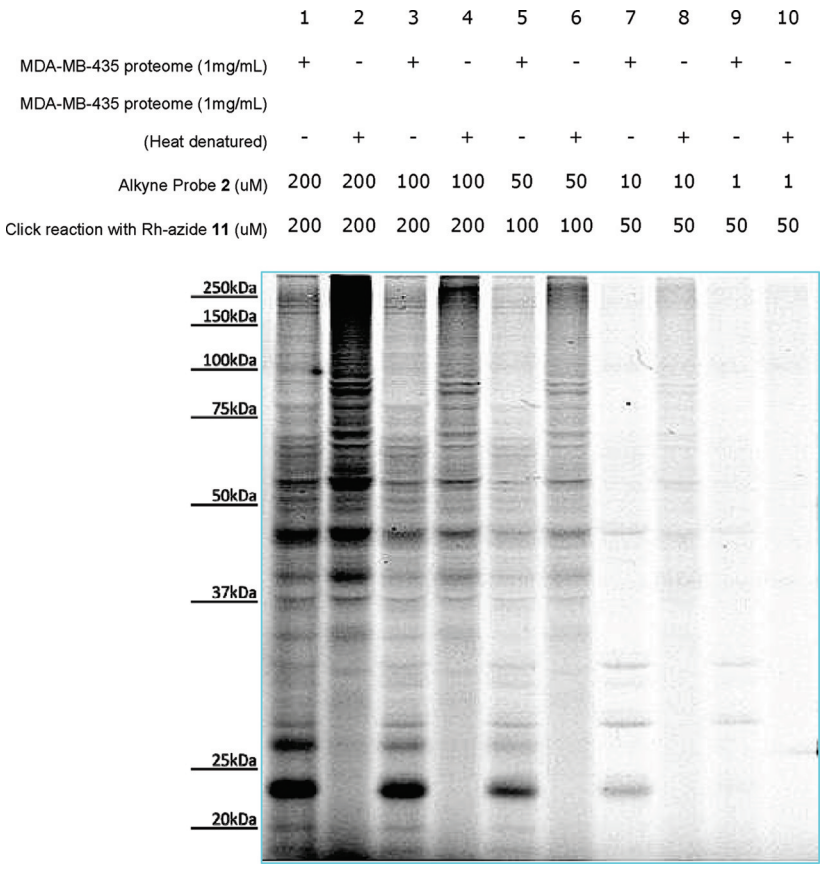

Figure 6. Labeling studies to ascertain effective probe concentrations (fluorescent gel image shown in gray scale). Probe concentrations were screened using MDA-MB-435 cancer cell extracts (soluble fraction) to identify concentrations that were effective for studies. Concentrations ranging from 1 to 200 nM were used to label the same amount of cell extracts with heat-denatured controls performed for each protein concentration. From fluorescence gel imaging results, probe concentrations of approximately 50 μM (lanes 5 and 6) were selected for other labeling studies. Please also see color fluorescence gel scans in Figure S2 of the Supporting Information.

experiments mirrored those of Figure 3 in that probe **3** bearing a longer linker yielded minimal labeling compared to **2**. These results further confirm the importance of linker length in probe design. Additionally, bifunctional lysine analogue **8a** lacking a PIP_n headgroup again appeared to label proteins in a manner different from that of probe **2**, which is likely attributable to nonspecific binding resulting from the hydrophobicity of this compound.

Proteomic Analysis for Probe-Based Characterization of Labeled Proteins Using MDA-MB-435 Cancer Cell Extracts. The initial phases of this research demonstrated that PIP_n activity probes are effective for labeling of protein binding targets. Following these results, we set out to apply these probes for proteomic analysis using MDA-MB-435 cell extracts to characterize protein binding targets. Because of its effectiveness in prior protein labeling studies, alkyne-PI(3,4,5)-P_3 probe **2** was selected for proteomics experiments, which were performed as described in the legend of Figure 5. Cell extracts were incubated with probe **2** and irradiated as described previously, followed by reaction with azido-biotin **12**. Subsequently, biotinylated probe-labeled proteins were separated from unlabeled proteins through streptavidin-based affinity chromatography. Enriched proteins were then digested into peptides using trypsin, and the resulting peptide mixture was analyzed by multidimensional liquid chromatography tandem mass spectrometry (LC/LC−MS/MS) using the Multidimensional Protein Identification Technology (MudPIT) technique.[45] Peptide sequences were determined using the SEQUEST algorithm[77] and organized and matched to the parent proteins using DTASelect.[78] Spectral counting, a semiquantitative measure of relative protein abundance, was used in this study to identify proteins enriched in the probe-labeled samples.[43,79,80] Additionally, control studies using lysine linker **8a** lacking a PIP_n headgroup or lacking any probe were performed side by side with these analyses to determine background enrichments.

From these proteomic experiments, 265 proteins were detected with significantly increased spectral counts in probe-labeled samples compared to controls. In these studies, three probe-labeled samples were run, and only those proteins that were observed in at least two of these runs and yielded at least two unique spectral counts were included. In addition, proteins that are known to be endogenously biotinylated, such as methylcrotonoyl-CoA carboxylase, were discounted. The resulting proteins are classified on the basis of the average number of spectral counts relative to controls in Table 1 (≥5-fold above control, 97 proteins) and Table 2 (2−5-fold above controls, 168 proteins). While 2−5-fold enrichments in probe-labeled samples (proteins in Table 2) represent relatively weak signals, it should be noted that a number of proteins that have previously been implicated as PI(3,4,5)P_3 binders appear in Table 2, which is further discussed below. This provides evidence that 2−5-fold enrichment is sufficient for identifying putative targets. Furthermore, modest enrichments are likely

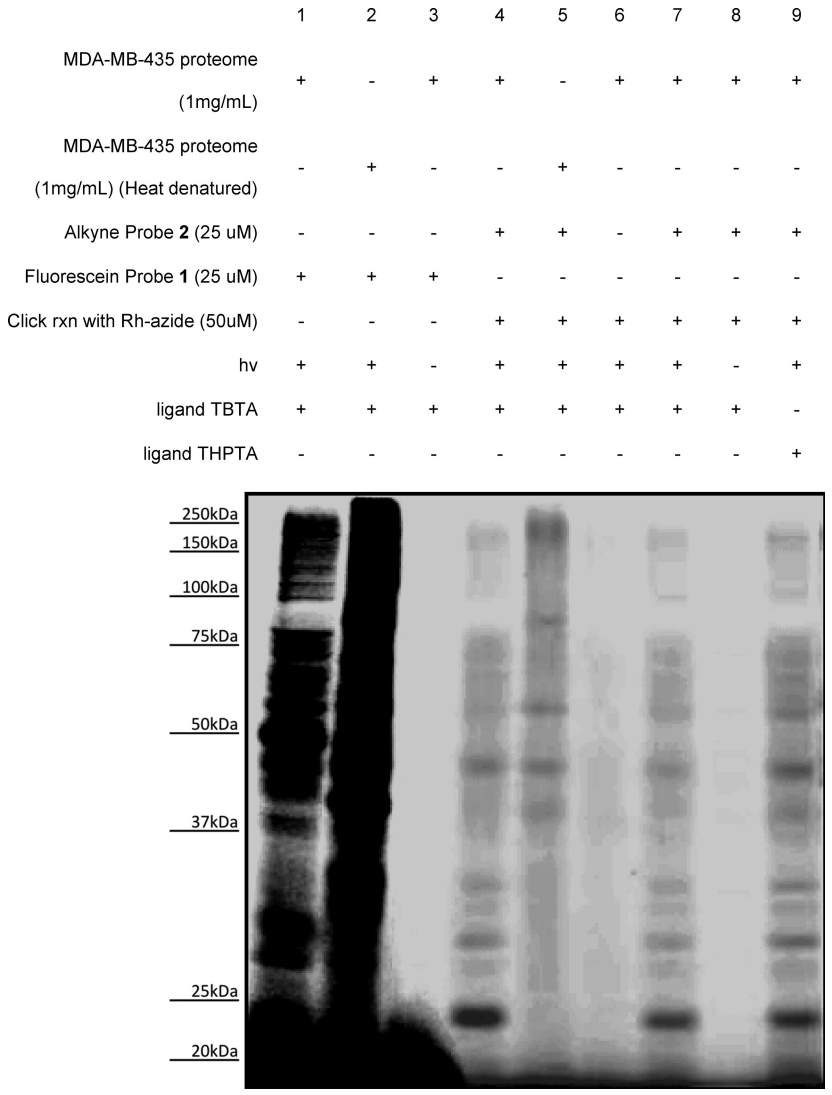

Figure 7. Labeling of the MDA-MB-435 soluble proteome using various conditions (fluorescent gel image shown in gray scale). Studies using fluorescein probe **1** resulted in significantly stronger labeling in the heat-denatured control (lane 2) compared to the normal study (lane 1), indicating that the presence of the fluorophore during labeling is problematic. Studies using probe **2** and postlabeling led to diminished labeling in the heat-denatured control (lane 5, when compared to lane 4). No probe (lane 6) and no light (lane 8) controls negated labeling, and click chemistry ligands TBTA (lane 7) and THPTA (lane 9) yielded similar results. Please also see color fluorescence gel scans in Figure S3 of the Supporting Information.

attributable to the low efficiencies commonly observed in photoaffinity labeling events, weak expression of certain protein targets, and/or nonspecific binding of proteins during streptavidin enrichment.

Of the total of 265 proteins that were oberved, many have been identified as PI(3,4,5)P_3-binding proteins in previous reports, including affinity chromatography studies. For example, 38 proteins were among the PI(3,4,5)P_3-binding proteins identified by Catimel and co-workers;[25] four proteins coincide with those detected by Dixon and co-workers,[30] and two proteins were also identified by Pasquali and co-workers.[24] Proteins that were previously observed in global proteomics screens are indicated with citations in Tables 1 and 2. In 2002, Krugmann and co-workers identified ARAP3 as a novel PI(3,4,5)P_3 binding receptor,[22] while in our studies, a protein from the same family, ARAP1, was identified, which was also observed by Dixon and co-workers.[30] Similary, while Dixon and co-workers reported eukaryotic translation initiation factor 4E, we found eukaryotic translation initiation factors 3E, 4H, 5A, and 6. Furthermore, a number of proteins that were detected contain conserved binding modules that are known to target PIP_ns. These included proteins bearing calponin homology (CH) (α-actinin-1 and -4, filamin-A and -B, MARE1, plectin, IQGA1, and β-spectrin-1), pleckstrin homology (PH) (ARAP1, β-spectrin-1, and SWP70), septin (septins 2, 7, and 9), 4.1 protein ezrin radixin moesin (FERM) (moesin and radixin), Huntington elongation factor 3 PR65/A TOR (HEAT) (2AAA and GCN1L), clathrin (clathrin heavy chain 1), and annexin (annexins A1 and A2) domains. One issue with this study that may or may not be general is that a number of known PI(3,4,5)P_3-binding proteins were not observed. This could result from multiple factors that are detailed in the Discussion.

In addition to known binding properties and domains, the identified proteins also possess many common functional themes, which are again in general agreement with the conserved roles that have emerged from other PIP_n binding studies. For example, PI(3,4,5)P_3 has commonly been implicated in the regulation of the actin cytoskeleton, and indeed, these studies

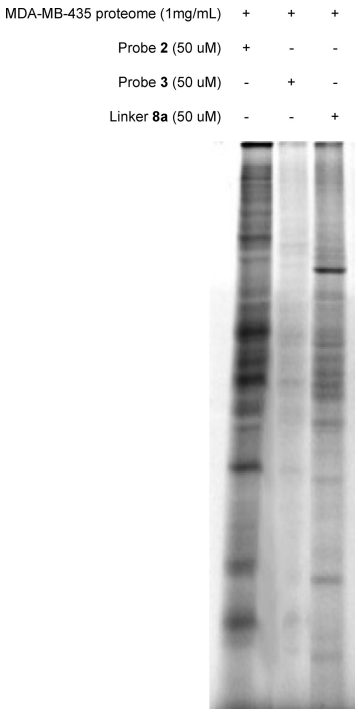

Figure 8. Analysis of the effect of probe linker length using MDA-MB-435 cancer cell extracts (fluorescent gel image). Labeling studies with probe **2** (shorter linker) yielded significantly enhanced labeling compared to that with probe **3**. Control compound **8a** lacking the PIP_n headgroup yielded minimal protein labeling of an orthogonal subset of proteins.

yielded at least 12 actin-binding proteins, such as gelsolin, twinfilin-2, β-spectrin, fructose-bisphosphate aldolase A, plectin, radixin, myosins, and filamins. Tables 1 and 2 also include at least 55 proteins involved in ATP binding (21%), seven proteins involved in GTP binding (dynamin-1-like protein, ERF3B, EF1A3, and septins 2, 7, and 9), nine proteins involved in protein transport (α-coatamer, IF5A1, exportin-2, importin-11, RAN, myosin-Ic, nucleophosmin, sequestosome-1, and transportin-3), three proteins involved in cell adhesion (leupaxin, PLAK, and LPP), and three proteins involved in signal transduction (filamin-B, leupaxin, and 2ABA). Finally, at least 86 of the labeled proteins participate in protein binding (32%), and many common enzymatic activities were present, including at least 29 hydrolases, 19 transferases, 13 oxido-reductases, 14 kinases, 9 isomerases, and 5 lyases.

Another point of interest involves the dependence of protein labeling results on the particular system that is being analyzed. In this case, the fact that studies were performed using a cancer cell line may lead to certain processes, such as actin skeleton regulation, being particularly represented because of disease-related upregulation. In future studies, we will seek to exploit the ability to use ABPP to identify proteomic variations by comparing profiles of normal cells with those associated with particular conditions, which has previously been performed for cancer,[37,81−83] malaria,[84,85] and obesity[86] cell lines. Finally, proteins detected during our studies that were not previously known to bind $PI(3,4,5)P_3$ offer putative new targets for this ligand. As is always the case with global proteomic approaches, further work is necessary to confirm specific binding interactions, but these techniques provide a highly efficient avenue for uncovering prospective targets. Furthermore, certain putative targets exhibit important ramifications for future studies. For example, in this study, the labeling of PARK7, associated with Parkinson's disease, opens up interesting possibilities and could be scrutinized further.

DISCUSSION

In this study, we designed, synthesized, and applied bifunctional activity-based probes corresponding to PIP_ns to label and identify protein targets of these critical ligands. Probes consisting of PIP_n headgroup analogues decorated with both a photoaffinity tag for cross-linking to bound proteins and a secondary tag for subsequent analysis were found to be effective for labeling protein targets. In particular, the use of an alkyne secondary tag followed by click chemistry provided a versatile approach for both in-gel fluorescence detection and biotin-based affinity purification that also minimized nonspecific protein labeling. The latter problem is likely caused by the bulky reporter groups that are present within the probe structure when click chemistry is not used for postlabeling. Initial studies involving the purified PH domain of Akt yielded effective labeling of this protein that was abrogated using competition binding, heat denaturation, no probe, and no light controls, indicating specific labeling resulting from a discrete binding interaction. The study of probes containing different linker lengths between the $PI(3,4,5)P_3$ headgroup and bifunctional tag indicated that a shorter linker (probe **2**) resulted in greatly enhanced protein labeling in this particular case. While this does not necessarily mean that the linker length in this probe is optimal, it does clearly show that the spacing of the photoaffinity group is critical for subsequent protein labeling. In fact, the ideal spacer length would likely vary depending upon the specific three-dimensional structure of the protein target and the proximity of residues. Nevertheless, there should be a range of distances in which cross-linking is feasible before the distance and flexibility of the photoaffinity tag become too great to allow significant protein labeling.

Following optimization of labeling studies and controls using cancer cell extracts, probe **2** was exploited for proteomic analysis for collective identification of protein targets from these samples, which resulted in the identification of 265 proteins. The inclusion of previously known $PI(3,4,5)P_3$ binding targets, proteins bearing conserved PIP_n-binding domains, and many proteins involved in processes associated with PIP_ns provides evidence that this approach is effective for detection of specific protein targets. As a result, the other proteins that were observed represent solid candidate target effectors for further study. It should also be noted that the described probe strategy may also pull down proteins that bind the soluble inositol phosphates (InsPs).[87,88] In this case, probe **2** could also be considered an analogue of inositol 1,3,4,5-tetrakisphosphate, in which the phosphate at position 1 has been modified for linkage via a phosphodiester, a linkage strategy that has previously been pursued to develop probes corresponding to the InsPs.[62−70] Ultimately, the binding properties of InsPs and PIP_ns are often difficult to differentiate because of their similar structures, and indeed, members of each family have been observed to compete for the same protein binding targets.[89−92]

One issue with this study is that a number of known $PI(3,4,5)P_3$-binding proteins were not observed. This could be due to a number of factors, including the nature of the probe structures employed for studies, challenges associated with the cross-linking of sufficient quantities of protein for detection, and the use of cell extracts for experiments. One aspect that will

affect the proteins that are observed pertains to the structure of the probe that is employed for protein labeling. Previous work has led to the categorization of PIP_n-binding domains on the basis of binding mode, as some proteins bind predominately to the phosphorylated *myo*-inositol headgroup (S-type proteins), others interact with the interfacial membrane region (I-type proteins), and finally a third binding mode involves substantial penetration of the protein into the hydrophobic membrane core (H-type proteins).[4] Because probe **2** corresponds to a soluble headgroup analogue, it would be expected that this compound would be more effective at labeling S-type proteins than H-type proteins. This effect can be seen in the data because proteins bearing domains that primarily target headgroups, such as the S-type ANTH and PH modules, were found, while those requiring membrane penetration, such as the H-type ENTH and PX domains, were not.

As discussed previously, soluble activity probes were expected to be beneficial for protein labeling studies to present the photoaffinity tag proximal to bound proteins and avoid nonspecific hydrophobic interactions. While this approach may limit the labeling of proteins that require the membrane environment for binding, it will be challenging to devise a single probe structure that will be effective for labeling the majority of PIP_n-binding proteins because of their diverse binding modes. Instead, multiple probes with different structural features will likely be necessary. The need for different structural probes has already been observed in affinity chromatography studies, where isolated beads and those associated with liposomes were found to pull out different and only mildly overlapping sets of proteins.[25] In future studies, we will pursue different probe structures to improve our understanding of the effect this has on proteins that are labeled. Because PIP_n-binding proteins exhibit a broad variation in binding mode in terms of headgroup−membrane binding, localization, multivalency, and requirements for other ligands, diverse probe strategies will likely be necessary to fully elucidate the complex scope of binding targets.

Successful photolabeling of proteins relies on a number of factors, including the amount of protein that is effectively labeled, the efficiency of cross-linking, and the placement of the photoaffinity tag in the proximity of residues on the bound protein. Low-abundance proteins are challenging to detect, which is compounded by the low cross-linking efficiencies commonly observed with photoaffinity groups. Furthermore, proteins should only be labeled when they are in the form in which ligand binding is activated, and lipid-binding proteins are tightly regulated in spatial and temporal manners. In addition, the ideal placement of the photoaffinity tag will likely vary for each protein target depending upon the three-dimensional arrangement of nearby residues in the binding domain. This represents a more general rationale for why it is unlikely that a single probe structure would be equally effective for labeling all target proteins. While this approach may not pull out every target, it nevertheless provides an efficient means for identifying a set of putative protein targets from highly complex samples. Finally, studies performed using cell extracts may not be ideal because they do not take place in the native environment inside the cell. A primary benefit of ABPP is that this strategy is amenable to analysis using live cells and organisms. Now that these initial PIP_n activity probes have proven to be effective for labeling and identifying target proteins, we are currently working on modifying probes and conditions to undertake studies in living samples.

■ ASSOCIATED CONTENT

Ⓢ Supporting Information

Procedures, characterization data, and color gel images. This material is available free of charge via the Internet at http://pubs.acs.org.

■ AUTHOR INFORMATION

Corresponding Author

*Phone: (865) 974-8658. Fax: (865) 974-9332. E-mail: mdbest@utk.edu.

■ ACKNOWLEDGMENTS

This work was made possible by funding from the National Science Foundation (CHE-0954297 for MDB) and the National Institutes of Health (R01 CA087660 for BFC and GM68849 for WC). We also thank Dr. Sherry Niessen from the The Center for Physiological Proteomics at The Scripps Research Institute for assistance with mass spectrometry-based proteomic studies.

■ REFERENCES

(1) Best, M. D., Zhang, H. L., and Prestwich, G. D. (2010) Inositol polyphosphates, diphosphoinositol polyphosphates and phosphatidylinositol polyphosphate lipids: Structure, synthesis, and development of probes for studying biological activity. *Nat. Prod. Rep. 27*, 1403−1430.

(2) Conway, S. J., and Miller, G. J. (2007) Biology-enabling inositol phosphates, phosphatidylinositol phosphates and derivatives. *Nat. Prod. Rep. 24*, 687−707.

(3) Lemmon, M. A. (2008) Membrane recognition by phospholipid-binding domains. *Nat. Rev. Mol. Cell Biol. 9*, 99−111.

(4) Cho, W., and Stahelin, R. V. (2005) Membrane-protein interactions in cell signaling and membrane trafficking. *Annu. Rev. Biophys. Biomol. Struct. 34*, 119−151.

(5) Di Paolo, G., and De Camilli, P. (2006) Phosphoinositides in cell regulation and membrane dynamics. *Nature 443*, 651−657.

(6) Pendaries, C., Tronchere, H., Plantavid, M., and Payrastre, B. (2003) Phosphoinositide signaling disorders in human diseases. *FEBS Lett. 546*, 25−31.

(7) Vicinanza, M., D'Angelo, G., Di Campli, A., and De Matteis, M. A. (2008) Phosphoinositides as regulators of membrane trafficking in health and disease. *Cell. Mol. Life Sci. 65*, 2833−2841.

(8) Wymann, M. P., and Schneiter, R. (2008) Lipid signalling in disease. *Nat. Rev. Mol. Cell Biol. 9*, 162−176.

(9) Assinder, S. J., Dong, Q. H., Kovacevic, Z., and Richardson, D. R. (2009) The TGF-β, PI3K/Akt and PTEN pathways: Established and proposed biochemical integration in prostate cancer. *Biochem. J. 417*, 411−421.

(10) Duronio, V. (2008) The life of a cell: Apoptosis regulation by the PI3K/PKB pathway. *Biochem. J. 415*, 333−344.

(11) Engelman, J. A., Luo, J., and Cantley, L. C. (2006) The evolution of phosphatidylinositol 3-kinases as regulators of growth and metabolism. *Nat. Rev. Genet. 7*, 606−619.

(12) Manning, B. D., and Cantley, L. C. (2007) AKT/PKB signaling: Navigating downstream. *Cell 129*, 1261−1274.

(13) Salmena, L., Carracedo, A., and Pandolfi, P. P. (2008) Tenets of PTEN tumor suppression. *Cell 133*, 403−414.

(14) Yuan, T. L., and Cantley, L. C. (2008) PI3K pathway alterations in cancer: Variations on a theme. *Oncogene 27*, 5497−5510.

(15) Stokoe, D., Stephens, L. R., Copeland, T., Gaffney, P. R. J., Reese, C. B., Painter, G. F., Holmes, A. B., McCormick, F., and Hawkins, P. T. (1997) Dual role of phosphatidylinositol-3,4,5-trisphosphate in the activation of protein kinase B. *Science 277*, 567−570.

(16) Katso, R., Okkenhaug, K., Ahmadi, K., White, S., Timms, J., and Waterfield, M. D. (2001) Cellular function of phosphoinositide

3-kinases: Implications for development, immunity, homeostasis, and cancer. *Annu. Rev. Cell Dev. Biol. 17*, 615−675.
(17) Maehama, T., and Dixon, J. E. (1998) The tumor suppressor, PTEN/MMAC1, dephosphorylates the lipid second messenger, phosphatidylinositol 3,4,5-trisphosphate. *J. Biol. Chem. 273*, 13375−13378.
(18) Samuels, Y., Wang, Z. H., Bardelli, A., Silliman, N., Ptak, J., Szabo, S., Yan, H., Gazdar, A., Powell, D. M., Riggins, G. J., Willson, J. K. V., Markowitz, S., Kinzler, K. W., Vogelstein, B., and Velculescu, V. E. (2004) High frequency of mutations of the PIK3CA gene in human cancers. *Science 304*, 554−554.
(19) Chow, L. M. L., and Baker, S. J. (2006) PTEN function in normal and neoplastic growth. *Cancer Lett. 241*, 184−196.
(20) Rao, V. R., Corradetti, M. N., Chen, J. A., Peng, J. R., Yuan, J. Y., Prestwich, G. D., and Brugge, J. S. (1999) Expression cloning of protein targets for 3-phosphorylated phosphoinositides. *J. Biol. Chem. 274*, 37893−37900.
(21) Painter, G. F., Thuring, J. W., Lim, Z. Y., Holmes, A. B., Hawkins, P. T., and Stephens, L. R. (2001) Synthesis and biological evaluation of a PtdIns(3,4,5)P-3 affinity matrix. *Chem. Commun.*, 645−646.
(22) Krugmann, S., Anderson, K. E., Ridley, S. H., Risso, N., McGregor, A., Coadwell, J., Davidson, K., Eguinoa, A., Ellson, C. D., Lipp, P., Manifava, M., Ktistakis, N., Painter, G., Thuring, J. W., Cooper, M. A., Lim, Z. Y., Holmes, A. B., Dove, S. K., Michell, R. H., Grewal, A., Nazarian, A., Erdjument-Bromage, H., Tempst, P., Stephens, L. R., and Hawkins, P. T. (2002) Identification of ARAP3, a novel PI3K effector regulating both Arf and Rho GTPases, by selective capture on phosphoinositide affinity matrices. *Mol. Cell 9*, 95−108.
(23) Lim, Z. Y., Thuring, J. W., Holmes, A. B., Manifava, M., and Ktistakis, N. T. (2002) Synthesis and biological evaluation of a PtdIns(4,5)P-2 and a phosphatidic acid affinity matrix. *J. Chem. Soc., Perkin Trans. 1*, 1067−1075.
(24) Pasquali, C., Bertschy-Meier, D., Chabert, C., Curchod, M. L., Arod, C., Booth, R., Mechtler, K., Vilbois, F., Xenarios, I., Ferguson, C. G., Prestwich, G. D., Camps, M., and Rommel, C. (2007) A chemical proteomics approach to phosphatidylinositol 3-kinase signaling in macrophages. *Mol. Cell. Proteomics 6*, 1829−1841.
(25) Catimel, B., Yin, M. X., Schieber, C., Condron, M., Patsiouras, H., Catimel, J., Robinson, D., Wong, L. S. M., Nice, E. C., Holmes, A. B., and Burgess, A. W. (2009) PI(3,4,5)P3 Interactome. *J. Proteome Res. 8*, 3712−3726.
(26) Catimel, B., Schleber, C., Condron, M., Patsiouras, H., Connolly, L., Catimel, J., Nice, E. C., Burgess, A. W., and Holmes, A. B. (2008) The PI(3,5)P2 and PI(4,5)P2 Interactomes. *J. Proteome Res. 7*, 5295−5313.
(27) Conway, S. J., Gardiner, J., Grove, S. J. A., Johns, M. K., Lim, Z.-Y., Painter, G. F., Robinson, D. E. J. E., Schieber, C., Thuring, J. W., Wong, L. S.-M., Yin, M.-X., Burgess, A. W., Catimel, B., Hawkins, P. T., Ktistakis, N. T., Stephens, L., and Holmes, A. B. (2010) Synthesis and biological investigation of phosphatidylinositol phosphate affinity probes. *Org. Biomol. Chem. 8*, 66−76.
(28) Tanaka, K., ImajohOhmi, S., Sawada, T., Shirai, R., Hashimoto, Y., Iwasaki, S., Kaibuchi, K., Kanaho, Y., Shirai, T., Terada, Y., Kimura, K., Nagata, S., and Fukui, Y. (1997) A target of phosphatidylinositol 3,4,5-trisphosphate with a zinc finger motif similar to that of the ADP-ribosylation-factor GTPase-activating protein and two pleckstrin homology domains. *Eur. J. Biochem. 245*, 512−519.
(29) Wang, D. S., Ching, T. T., St Pyrek, J., and Chen, C. S. (2000) Biotinylated phosphatidylinositol 3,4,5-trisphosphate as affinity ligand. *Anal. Biochem. 280*, 301−307.
(30) Dixon, M. J., Gray, A., Boisvert, F. M., Agacan, M., Morrice, N. A., Gourlay, R., Leslie, N. R., Downes, C. P., and Batty, I. H. (2011) A screen for novel phosphoinositide 3-kinase effector proteins. *Mol. Cell. Proteomics 10*, M110.003178.
(31) Zhu, H., Bilgin, M., Bangham, R., Hall, D., Casamayor, A., Bertone, P., Lan, N., Jansen, R., Bidlingmaier, S., Houfek, T., Mitchell, T., Miller, P., Dean, R. A., Gerstein, M., and Snyder, M. (2001) Global analysis of protein activities using proteome chips. *Science 293*, 2101−2105.
(32) Cravatt, B. F., Wright, A. T., and Kozarich, J. W. (2008) Activity-based protein profiling: From enzyme chemistry. *Annu. Rev. Biochem. 77*, 383−414.
(33) Gubbens, J., Ruijter, E., de Fays, L. E. V., Damen, J. M. A., de Kruijff, B., Slijper, M., Rijkers, D. T. S., Liskamp, R. M. J., and de Kroon, A. (2009) Photocrosslinking and click chemistry enable the specific detection of proteins interacting with phospholipids at the membrane interface. *Chem. Biol. 16*, 3−14.
(34) Gubbens, J., and de Kroon, A. (2010) Proteome-wide detection of phospholipid-protein interactions in mitochondria by photocrosslinking and click chemistry. *Mol. BioSyst. 6*, 1751−1759.
(35) Tully, S. E., and Cravatt, B. F. (2010) Activity-based probes that target functional subclasses of phospholipases in proteomes. *J. Am. Chem. Soc. 132*, 3264−3265.
(36) Gong, D., Bostic, H. E., Smith, M. D., and Best, M. D. (2009) Synthesis of modular headgroup conjugates corresponding to all seven phosphatidylinositol polyphosphate isomers for convenient probe generation. *Eur. J. Org. Chem.*, 4170−4179.
(37) Speers, A. E., and Cravatt, B. F. (2004) Profiling enzyme activities in vivo using click chemistry methods. *Chem. Biol. 11*, 535−546.
(38) Hong, V., Presolski, S. I., Ma, C., and Finn, M. G. (2009) Analysis and Optimization of Copper-Catalyzed Azide-Alkyne Cycloaddition for Bioconjugation. *Angew. Chem., Int. Ed. 48*, 9879−9883.
(39) Manna, D., Albanese, A., Park, W. S., and Cho, W. (2007) Mechanistic basis of differential cellular responses of phosphatidylinositol 3,4-bisphosphate- and phosphatidylinositol 3,4,5-trisphosphate-binding pleckstrin homology domains. *J. Biol. Chem. 282*, 32093−32105.
(40) Smith, M. D., Gong, D. H., Sudhahar, C. G., Reno, J. C., Stahelin, R. V., and Best, M. D. (2008) Synthesis and convenient functionalization of azide-labeled diacylglycerol analogues for modular access to biologically active lipid probes. *Bioconjugate Chem. 19*, 1855−1863.
(41) Guichard, G., Fournel, S., Trouche, N., and Wieckowski, S. (2008) Preparation of new multimeric molecules, particularly CD40 ligands, for use in the preparation of drugs.
(42) Speers, A. E., Adam, G. C., and Cravatt, B. F. (2003) Activity-based protein profiling in vivo using a copper(I)-catalyzed azide-alkyne [3 + 2] cycloaddition. *J. Am. Chem. Soc. 125*, 4686−4687.
(43) Jessani, N., Niessen, S., Wei, B. Q. Q., Nicolau, M., Humphrey, M., Ji, Y. R., Han, W. S., Noh, D. Y., Yates, J. R., Jeffrey, S. S., and Cravatt, B. F. (2005) A streamlined platform for high-content functional proteomics of primary human specimens. *Nat. Methods 2*, 691−697.
(44) Peng, J. M., Elias, J. E., Thoreen, C. C., Licklider, L. J., and Gygi, S. P. (2003) Evaluation of multidimensional chromatography coupled with tandem mass spectrometry (LC/LC-MS/MS) for large-scale protein analysis: The yeast proteome. *J. Proteome Res. 2*, 43−50.
(45) Washburn, M. P., Wolters, D., and Yates, J. R. (2001) Large-scale analysis of the yeast proteome by multidimensional protein identification technology. *Nat. Biotechnol. 19*, 242−247.
(46) Dorman, G., and Prestwich, G. D. (2000) Using photolabile ligands in drug discovery and development. *Trends Biotechnol. 18*, 64−77.
(47) Ballell, L., Alink, K. J., Slijper, M., Versluis, C., Liskamp, R. M. J., and Pieters, R. J. (2005) A new chemical probe for proteomics of carbohydrate-binding proteins. *ChemBioChem 6*, 291−295.
(48) Ballell, L., van Scherpenzeel, M., Buchalova, K., Liskamp, R. M. J., and Pieters, R. J. (2006) A new chemical probe for the detection of the cancer-linked galectin-3. *Org. Biomol. Chem. 4*, 4387−4394.
(49) van Scherpenzeel, M., van der Pot, M., Arnusch, C. J., Liskamp, R. M. J., and Pieters, R. J. (2007) Detection of galectin-3 by novel peptidic photoprobes. *Bioorg. Med. Chem. Lett. 17*, 376−378.

(50) Best, M. D., Rowland, M. M., and Bostic, H. E. Exploiting bioorthogonal chemistry to elucidate protein-lipid binding interactions and other biological roles of phospholipids. *Acc. Chem. Res. 44*, 686–698.
(51) Sletten, E. M., and Bertozzi, C. R. (2009) Bioorthogonal chemistry: Fishing for selectivity in a sea of functionality. *Angew. Chem., Int. Ed. 48*, 6974–6998.
(52) Best, M. D. (2009) Click chemistry and bioorthogonal reactions: Unprecedented selectivity in the labeling of biological molecules. *Biochemistry 48*, 6571–6584.
(53) Ferguson, K. M., Lemmon, M. A., Schlessinger, J., and Sigler, P. B. (1995) Structure of the high-affinity complex of inositol trisphosphate with a phospholipase-C pleckstrin homology domain. *Cell 83*, 1037–1046.
(54) Garcia, P., Gupta, R., Shah, S., Morris, A. J., Rudge, S. A., Scarlata, S., Petrova, V., McLaughlin, S., and Rebecchi, M. J. (1995) The pleckstrin homology domain of phospholipase C-δ_1 binds with high affinity to phosphatidylinositol 4,5-bisphosphate in bilayer membranes. *Biochemistry 34*, 16228–16234.
(55) Hirose, K., Kadowaki, S., Tanabe, M., Takeshima, H., and Iino, M. (1999) Spatiotemporal dynamics of inositol 1,4,5-trisphosphate that underlies complex Ca^{2+} mobilization patterns. *Science 284*, 1527–1530.
(56) Kavran, J. M., Klein, D. E., Lee, A., Falasca, M., Isakoff, S. J., Skolnik, E. Y., and Lemmon, M. A. (1998) Specificity and promiscuity in phosphoinositide binding by pleckstrin homology domains. *J. Biol. Chem. 273*, 30497–30508.
(57) Lemmon, M. A., Ferguson, K. M., Obrien, R., Sigler, P. B., and Schlessinger, J. (1995) Specific and high-affinity binding of inositol phosphates to an isolated pleckstrin homology domain. *Proc. Natl. Acad. Sci. U.S.A. 92*, 10472–10476.
(58) Prestwich, G. D. (1996) Touching all the bases: Synthesis of inositol polyphosphate and phosphoinositide affinity probes from glucose. *Acc. Chem. Res. 29*, 503–513.
(59) Gu, Q. M., and Prestwich, G. D. (1996) Synthesis of phosphotriester analogues of the phosphoinositides PtdIns(4,5)P-2 and PtdIns(3,4,5)P-3. *J. Org. Chem. 61*, 8642–8647.
(60) Painter, G. F., Grove, S. J. A., Gilbert, I. H., Holmes, A. B., Raithby, P. R., Hill, M. L., Hawkins, P. T., and Stephens, L. (1999) General synthesis of 3-phosphorylated myo-inositol phospholipids and derivatives. *J. Chem. Soc., Perkin Trans. 1*, 923–935.
(61) Kubiak, R. J., and Bruzik, K. S. (2003) Comprehensive and uniform synthesis of all naturally occurring phosphorylated phosphatidylinositols. *J. Org. Chem. 68*, 960–968.
(62) Henne, V., Mayr, G. W., Grabowski, B., Koppitz, B., and Soling, H. D. (1988) Semisynthetic derivatives of inositol 1,4,5-trisphosphate substituted at the 1-phosphate group: Effects on calium release from permeabilized guinea-pig parotid acinar cells and comparison with binding to alolase-A. *Eur. J. Biochem. 174*, 95–101.
(63) Dorman, G., Chen, J., and Prestwich, G. D. (1995) Synthesis of D-myo-P-1-(O-aminopropyl)-inositol-1,4,5-trisphosphate affinity probes from α-D-glucose. *Tetrahedron Lett. 36*, 8719–8722.
(64) Inoue, T., Kikuchi, K., Hirose, K., Iino, M., and Nagano, T. (1999) Synthesis and evaluation of 1-position-modified inositol 1,4,5-trisphosphate analogs. *Bioorg. Med. Chem. Lett. 9*, 1697–1702.
(65) Marecek, J. F., Estevez, V. A., and Prestwich, G. D. (1992) New tetherable derivatives of *myo*-inositol 2,4,5-trisphosphates and 1,3,4-trisphosphates. *Carbohydr. Res. 234*, 65–73.
(66) Nakanishi, W., Kikuchi, K., Inoue, T., Hirose, K., Iino, M., and Nagano, T. (2002) Hydrophobic modifications at 1-phosphate of inositol 1,4,5-trisphosphate analogues enhance receptor binding. *Bioorg. Med. Chem. Lett. 12*, 911–913.
(67) Olszewski, J. D., Dorman, G., Elliott, J. T., Hong, Y., Ahern, D. G., and Prestwich, G. D. (1995) Tethered benzophenone reagents for the synthesis of photoactivatable ligands. *Bioconjugate Chem. 6*, 395–400.
(68) Prestwich, G. D., Marecek, J. F., Mourey, R. J., Theibert, A. B., Ferris, C. D., Danoff, S. K., and Snyder, S. H. (1991) Tethered IP3: Synthesis and biochemical applications of the 1-*O*-(3-aminopropyl) ester of inositol 1,4,5-trisphosphate. *J. Am. Chem. Soc. 113*, 1822–1825.
(69) Schafer, R., Nehlssahabandu, M., Grabowsky, B., Dehlingerkremer, M., Schulz, I., and Mayr, G. W. (1990) Synthesis and application of photoaffinity analogs of inositol 1,4,5-trisphosphate selectively substituted at the 1-phosphate group. *Biochem. J. 272*, 817–825.
(70) Tegge, W., and Ballou, C. E. (1992) Syntheses of D-*myo*-inositol 1,4,5-trisphosphate affinity ligands. *Carbohydr. Res. 230*, 63–77.
(71) Smith, M. D., Sudhahar, C. G., Gong, D., Stahelin, R. V., and Best, M. D. (2009) Modular synthesis of biologically active phosphatidic acid probes using click chemistry. *Mol. BioSyst. 5*, 962–972.
(72) Frech, M., Andjelkovic, M., Ingley, E., Reddy, K. K., Falck, J. R., and Hemmings, B. A. (1997) High affinity binding of inositol phosphates and phosphoinositides to the pleckstrin homology domain of RAC protein kinase B and their influence on kinase activity. *J. Biol. Chem. 272*, 8474–8481.
(73) James, S. R., Downes, C. P., Gigg, R., Grove, S. J. A., Holmes, A. B., and Alessi, D. R. (1996) Specific binding of the Akt-1 protein kinase to phosphatidylinositol 3,4,5-trisphosphate without subsequent activation. *Biochem. J. 315*, 709–713.
(74) Baker, J. G., Middleton, R., Adams, L., May, L. T., Briddon, S. J., Kellam, B., and Hill, S. J. (2010) Influence of fluorophore and linker composition on the pharmacology of fluorescent adenosine A_1 receptor ligands. *Br. J. Pharmacol. 159*, 772–786.
(75) Wang, Q., Chan, T. R., Hilgraf, R., Fokin, V. V., Sharpless, K. B., and Finn, M. G. (2003) Bioconjugation by copper(I)-catalyzed azide-alkyne [3 + 2] cycloaddition. *J. Am. Chem. Soc. 125*, 3192–3193.
(76) Chan, T. R., Hilgraf, R., Sharpless, K. B., and Fokin, V. V. (2004) Polytriazoles as copper(I)-stabilizing ligands in catalysis. *Org. Lett. 6*, 2853–2855.
(77) Yates, J. R. III, Eng, J. K., McCormack, A. L., and Schieltz, D. (1995) Method to correlate tandem mass-spectra of modified peptides to amino-acid sequences in the protein database. *Anal. Chem. 67*, 1426–1436.
(78) Tabb, D. L., McDonald, W. H., and Yates, J. R. (2002) DTASelect and contrast: Tools for assembling and comparing protein identifications from shotgun proteomics. *J. Proteome Res. 1*, 21–26.
(79) Zybailov, B., Coleman, M. K., Florens, L., and Washburn, M. P. (2005) Correlation of relative abundance ratios derived from peptide ion chromatograms and spectrum counting for quantitative proteomic analysis using stable isotope labeling. *Anal. Chem. 77*, 6218–6224.
(80) Usaite, R., Wohlschlegel, J., Venable, J. D., Park, S. K., Nielsen, J., Olsson, L., and Yates, J. R. (2008) Characterization of global yeast quantitative proteome data generated from the wild-type and glucose repression *Saccharomyces cerevisiae* strains: The comparison of two quantitative methods. *J. Proteome Res. 7*, 266–275.
(81) Chiang, K. P., Niessen, S., Saghatelian, A., and Cravatt, B. F. (2006) An enzyme that regulates ether lipid signaling pathways in cancer annotated by multidimensional profiling. *Chem. Biol. 13*, 1041–1050.
(82) Jessani, N., Liu, Y. S., Humphrey, M., and Cravatt, B. F. (2002) Enzyme activity profiles of the secreted and membrane proteome that depict cancer cell invasiveness. *Proc. Natl. Acad. Sci. U.S.A. 99*, 10335–10340.
(83) Paulick, M. G., and Bogyo, M. (2008) Application of activity-based probes to the study of enzymes involved in cancer progression. *Curr. Opin. Genet. Dev. 18*, 97–106.
(84) Greenbaum, D. C., Baruch, A., Grainger, M., Bozdech, Z., Medzihradszky, K. F., Engel, J., DeRisi, J., Holder, A. A., and Bogyo, M. (2002) A role for the protease falcipain 1 in host cell invasion by the human malaria parasite. *Science 298*, 2002–2006.
(85) Arastu-Kapur, S., Ponder, E. L., Fonovic, U. P., Yeoh, S., Yuan, F., Fonovic, M., Grainger, M., Phillips, C. I., Powers, J. C., and Bogyo, M. (2008) Identification of proteases that regulate erythrocyte rupture by the malaria parasite *Plasmodium falciparum*. *Nat. Chem. Biol. 4*, 203–213.

(86) Barglow, K. T., and Cravatt, B. F. (2004) Discovering disease-associated enzymes by proteome reactivity profiling. *Chem. Biol. 11*, 1523−1531.
(87) Irvine, R. F. (2005) Inositide evolution: Towards turtle domination? *J. Physiol. 566*, 295−300.
(88) Irvine, R. F., and Schell, M. J. (2001) Back in the water: The return of the inositol phosphates. *Nat. Rev. Mol. Cell Biol. 2*, 327−338.
(89) Razzini, G., Berrie, C. P., Vignati, S., Broggini, M., Mascetta, G., Brancaccio, A., and Falasca, M. (2000) Novel functional PI 3-kinase antagonists inhibit cell growth and tumorigenicity in human cancer cell lines. *FASEB J. 14*, 1179−1187.
(90) Piccolo, E., Vignati, S., Maffucci, T., Innominato, P. F., Riley, A. M., Potter, B. V. L., Pandolfi, P. P., Broggini, M., Iacobelli, S., Innocenti, P., and Falasca, M. (2004) Inositol pentakisphosphate promotes apoptosis through the PI3-K/Akt pathway. *Oncogene 23*, 1754−1765.
(91) Riley, A. M., Guedat, P., Schlewer, G., Spiess, B., and Potter, B. V. L. (1998) A conformationally restricted cyclic phosphate analogue of inositol trisphosphate: Synthesis and physicochemical properties.
J. Org. Chem. 63, 295−305.
(92) Maffucci, T., Piccolo, E., Cumashi, A., Iezzi, M., Riley, A. M., Saiardi, A., Godage, H. Y., Rossi, C., Broggini, M., Iacobelli, S., Potter, B. V. L., Innocenti, P., and Falasca, M. (2005) Inhibition of the phosphatidylinositol 3-kinase/Akt pathway by inositol pentakisphosphate results in antiangiogenic and antitumor effects. *Cancer Res. 65*, 8339−8349.